Chapter 1

General Introduction

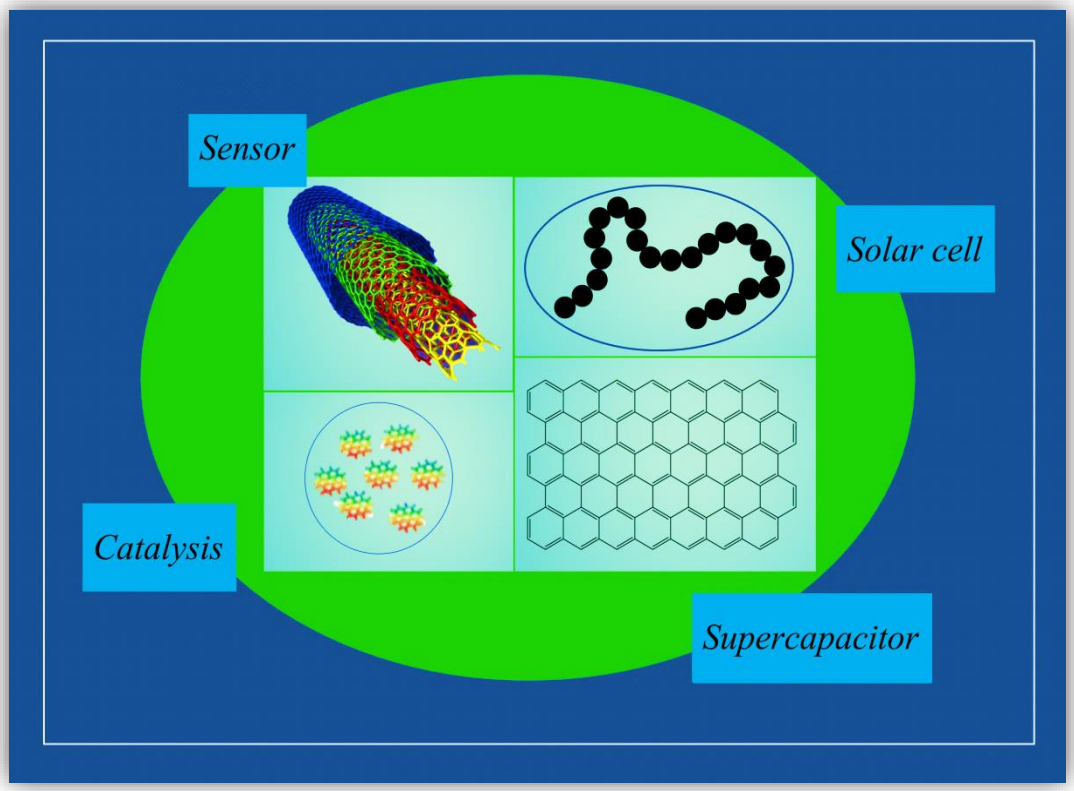

The motivation for the present investigation on carbon based nanomaterials is described in this chapter with a brief discussion on their potential applications in sensor, solar cell, supercapacitor and catalysis.

1.1 Motivation

Nanotechnology is an emerging multi-disciplinary technology that has revolutionized the existing traditional technologies. The National Nanotechnology Initiative defines nanotechnology as *"the understanding and control of matter at the nanoscale, at dimensions between approximately 1 and 100 nanometers, where unique phenomena enable novel applications"*[1]. When the size of any material is reduced to less than 100 nm in at least one dimension, it leads to changes in their fundamental physical properties. This concept was envisioned by R. P. Feynman back in 1959 when he delivered his famous lecture at Caltech titled *"There's Plenty of Room at the Bottom"*[2]. Later on, the pioneering works of K. E. Drexler published in the form of two books in 1986 and 1992 popularized the term "*nanotechnology*" [3]. Around the same time, carbon nanostructures were just been discovered, which further solidified the concept of nanotechnology. It can also be said that nanotechnology gave a new life to an old material: **carbon**.

By the mid-1980s, the field of carbon in terms of understanding their structure and properties, as well as their technological applications seemed to be saturated, and researchers were moving away from it. However, the discovery of Buckminsterfullerene by H. W. Kroto (at University of Sussex, UK),R. F. Curl, Jr. and R. E. Smalley(at Rice University, USA) in 1985 generated renewed interest in carbon [4]. For their discovery, the trio also received the Nobel Prize in 1996. The subsequent discovery of carbon nanotubes (CNTs) by S. Iijima in 1991 [5] and isolation of graphene by exfoliation of graphite by K. S. Novoselov, A. K. Geim and co-workers in 2004 [6] truly ushered in the new era of carbon based research that continues till date. For "groundbreaking experiments regarding the two-dimensional material graphene", A. K. Geim and K. Novoselov were awarded the Nobel Prize in 2010. Commensurate with the experimental and theoretical research on these new forms of carbon including graphene and carbon dots, developments are being made in varied areas ranging from energy [7,8] and electronics [9,10] to biomedical applications [11,12] and so on.

The motivation for this study is to develop carbon nanostructures and their composites, for potential applications in four diverse areas: sensors, solar cells, supercapacitors and anode catalysis in direct methanol fuel cell (DMFC).

1.2 Carbon

Carbon is one of the few elements known by human civilizations for millennia. The word carbon comes from the Latin word *"carbo*" meaning charcoal. The earliest use of carbon can be dated back to ~ 30,000 years ago when charcoal and carbon black were used for cave paintings **(Figure 1.1)**. There are other evidences of use of carbon throughout the history, e.g., reduction of metal ores by charcoal (8,500 B.C.), the Hindu sage Panningrishee invented the

Indian ink (carbon black) (3,500 B.C.), Egyptians used charcoal powder as medicine (1,500 B.C.), the Bible was printed by Johannes Gutenberg with printer's ink (carbon black) (1456 A.D.), and many others [13].

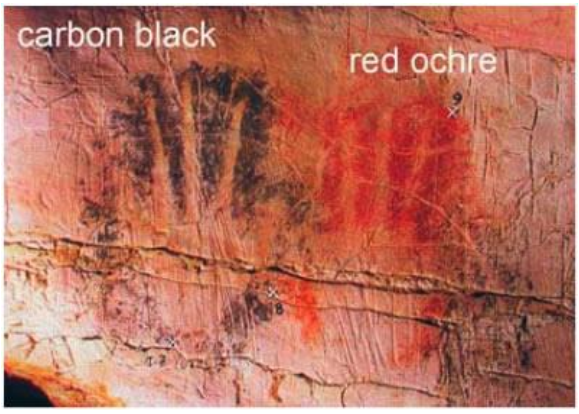

Figure 1.1 Paleolithic art in the Roucadour cave, France (28,000-25,000 B.P.) [14].

Carbon is a group 14 element represented by the symbol "C" and atomic number 6, having ground state electronic configuration of $1s^2 2s^2 2p^2$. Each carbon atom can form four covalent bonds by sharing its valence electrons with neighboring atoms. Due to the unique property of carbon to bind to itself as well as to almost all the other elements, it can form virtually limitless number of organic compounds. Graphite and diamond are the two earliest discovered naturally occurring allotropes of carbon. And they remained the only known carbon allotropes for a long time until the discovery of fullerenes. This discovery marked the commencement of a new age of synthetic allotropes of carbon.

1.2.1 Naturally occurring allotropes of carbon

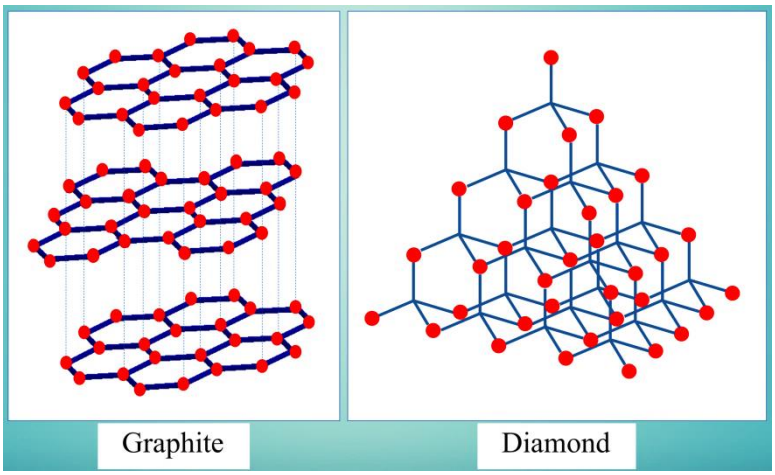

Figure 1.2 Atomic arrangements of graphite and diamond.

1.2.1.1 Graphite

Graphite is a soft material, black/gray in color. The word graphite was coined in 1789 by a German geologist A. G. Werner from the Greek word "*graphein*", meaning to write or draw. Graphite has a three-dimensional layered hexagonal structure**(Figure 1.2)**. Within the layers, the bonding is covalent with sp^2 hybridization, wherein one *s* orbital two *p* orbitals mix to give three sp^2 hybridized orbitals. The electrons in the remaining one *p* orbital behave like free electrons, and contribute to its conducting nature, thus making graphite a semi-metal. Meanwhile, the hexagonal layers are connected parallel to each other by van der Waals forces, with an inter-planar distance of 0.335 nm [15].

1.2.1.2 Diamond

Diamond gets its name from the ancient Greek word "*adamas*" meaning invincible. It is the sp^3 hybridized form of carbon. Each carbon atom is surrounded by four other atoms by covalent bonds, forming a strong three-dimensional tetrahedral structure with all the bonds having 0.154 nm length and equal bond angle of 109.4° **(Figure 1.2)** [16]. The structure, together with a highly directed charge density makes diamond the hardest natural material. It predominantly exists in face-cantered cubic form. Diamond is a good thermal conductor but it is electrically non-conducting.

1.2.2 Synthetic allotropes of carbon

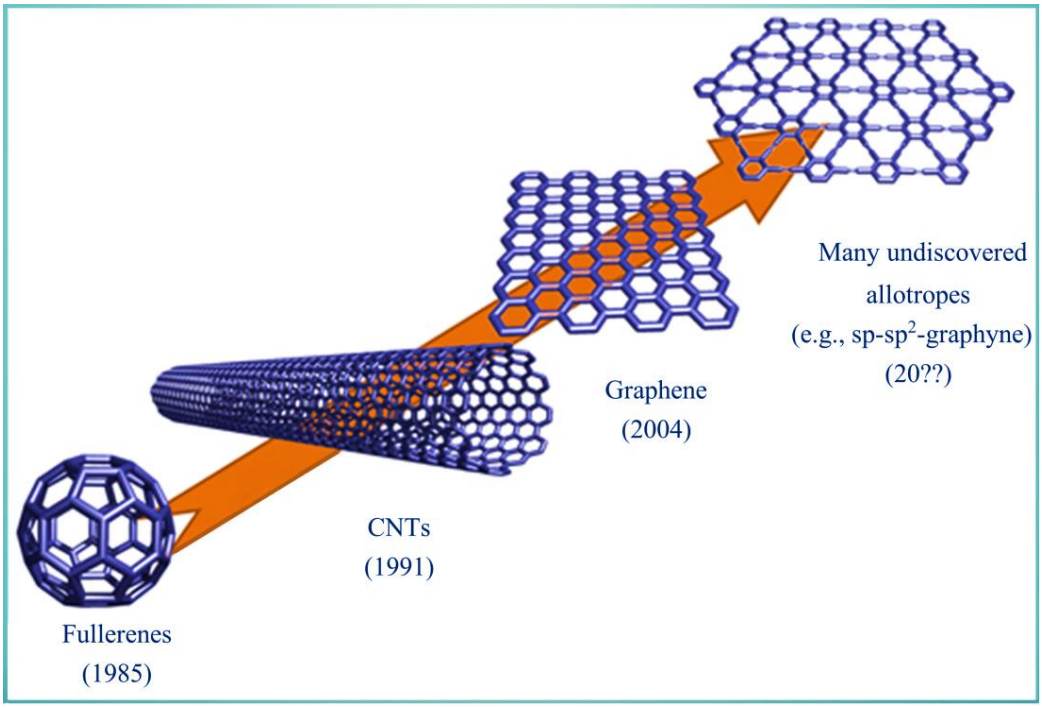

Figure 1.3 Evolution of synthetic carbon allotropes [17].

1.2.2.1 Fullerenes

Fullerenes are a class of molecules composed exclusively of carbon, existing as closed hollow cages, made of interconnected pentagonal and hexagonal rings similar to a football. Since all the dimensions of a fullerene are restricted to nanoscale, they are considered as zero-dimensional molecules and form the foundation for low dimensional carbon nanostructures. The most prominent fullerene C_{60}, which consists of 60 carbon atoms as the subscript implies, is also known as the *Buckminsterfullerene* or the *Bucky ball*. It was named after the American architect Buckminster Fuller who designed geodesic domes in the 1960s. Among these, the Montreal Biosphere designed by him in 1967 is shown in **Figure 1.4.** Structurally,C_{60} is composed of 12 pentagons and 20 hexagons.

Figure 1.4 The Montreal Biosphere designed by Buckminster Fuller in 1967.

The first successful synthesis of C_{60} in macroscopic scale by W. Kratschmer and co-workers [18] provided the breakthrough for rapid development in the field of fullerenes, not just C_{60}, but also others having carbon atoms ranging from 16 to hundreds. Theoretically, all C_{20+2F} structures are possible, where $F \neq 1$ and $F \geq 0$ [19]. Other popular examples of fullerenes include C_{70}, C_{76}, C_{78}, C_{84} and C_{90} [20].

Synthesis of fullerenes predominantly involves the generation of a carbon-rich vapor or plasma by any of the methods listed below [21–25]:

(i) laser vaporization of graphite,

(ii) electric arc heating of graphite,

(iii) resistive arc heating of carbon rods,

(iv) laser irradiation of polyaromatic hydrocarbons (PAHs), etc

1.2.2.2 Carbon nanotubes

CNTs are a unique member of the family of carbon nanostructures that normally have a length to diameter ratio of 1000 or more, hence considered as one-dimensional nanostructures. CNTs are renowned for their high strength. Bending tests conducted on individual CNTs *in situ* in a transmission electron microscope (TEM), resulted in a Young's modulus value of 0.9 TPa[26]. The tensile strength of CNTs is at least 117 times more than that of steel and 30 times than that of Kevlar, and their strain at break is 13.7% [27]. Their extraordinary strength can be accounted for by the presence of strong interlocking C-C covalent bonds, and also the fact that each CNT is one large molecule. This means that they do not have any grain boundaries that exist in steel and other materials. CNTs also possess high thermal conductivity. Instead of movement of electrons as dominant pathway to conduct heat (as metals do), CNTs conduct heat by lattice vibrations or *phonons* (discrete quanta of vibrations) [28], considered as energy carriers. The carbon atoms, in addition to the sp^2 hybridized C-C bonds, also wriggle around and transmit heat throughout the nanotube, which is further aided by the stiffness of the C-C bonds and a seamless hexagonal network. *Ballistic conduction* is another benefit of the CNT structure and dimensionality. When conduction occurs through a material without significant resistance caused by scattering, it is called a *ballistic conductor*. It occurs when the mean free path is longer than the CNT length, and the wavelength of the dominant phonon is smaller than the diameter of the CNT. The electrical properties of CNTs are particularly interesting, which vary from metallic to semi-conductors with different band-gaps. This is determined by the type of the nanotube, discussed in detail in the following sections.

CNTs are divided into two main categories.

(i) Single-walled carbon nanotubes (SWCNTs).

A SWCNT can simply be defined as a rolled-up graphene sheet. But depending on the way that graphene sheet is rolled, SWCNTs can be divided into three configurations: zig-zag, chiral and armchair **(Figure 1.5)**.

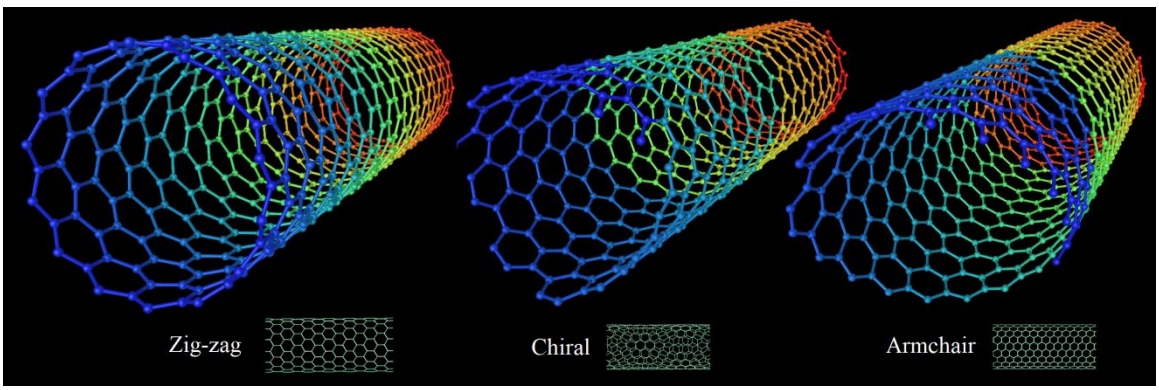

Figure 1.5 Three different types of SWCNT configurations [29].

(ii) Multi-walled carbon nanotubes (MWCNTs).

A MWCNT can be considered as a collection of concentric SWCNTs **(Figure 1.6)**.The distance between two tubes is approximately equal to the distance between two graphene layers in graphite (i.e., 0.335 nm. MWCNTs are almost always metallic in nature. In contrast to SWCNTs, MWCNTs possess relatively higher electrical conductivity and higher surface area. It is also easier to synthesize MWCNTs than SWCNTs.

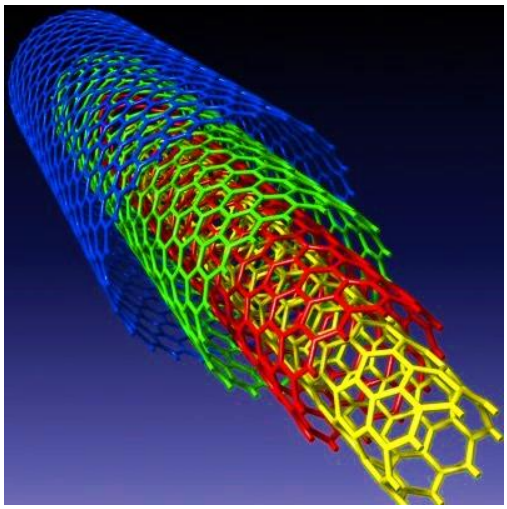

Figure 1.6 Structure of a MWCNT [30].

CNTs are generally produced by the three main techniques:

(a) *Arc discharge.* Carbon vapor is created by an arc discharge between two carbon electrodes. The carbon from the negative electrode sublimates due to high temperature caused by the discharge. CNTs self-assemble from this carbon vapor [31].

(b) *Chemical vapor deposition (CVD)*. A catalyst material is placed in a tubular reactor and heated to 600-1200 °C. A carbon containing gas, like methane or acetylene, is then slowly introduced. The gas is decomposed by the catalyst to free-up carbon atoms, which recombine to form CNTs [32].

(c) *Laser ablation.* A high power laser beam is impinged on a piece of graphite. CNTs are formed from the carbon vapor [33].

1.2.2.3 Graphene

Graphene is a single atom thick layer of sp^2 hybridized carbons with a honeycomb lattice that exhibits exceptional crystal and electronic properties. Graphitic materials of all other dimensionalities (like zero-dimensional fullerene, one-dimensional CNT and three-dimensional graphite or graphene aerogel, etc.) can be built from this basic two-dimensional building block **(Figure 1.7)**.

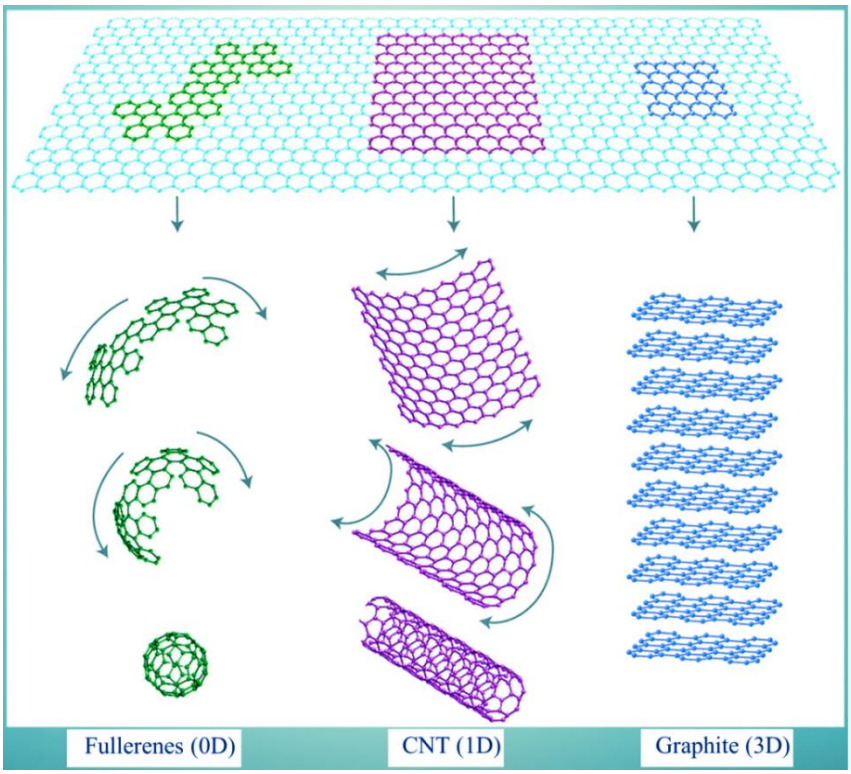

Figure 1.7 2D graphene as a building block for 0D fullerene, 1D CNT and 3D graphite [34].

A single layer graphene acts as a *zero-gap semi-conductor* (or a *zero-band overlap semi-metal*). If the crystal structure of graphene is assumed as two equivalent triangular sub-lattices, then hopping of the charge carriers between them leads to the formation of two energy bands, that touch each other at singularity points (*K* and *K'* points or Dirac points)**(Figure 1.8)**.

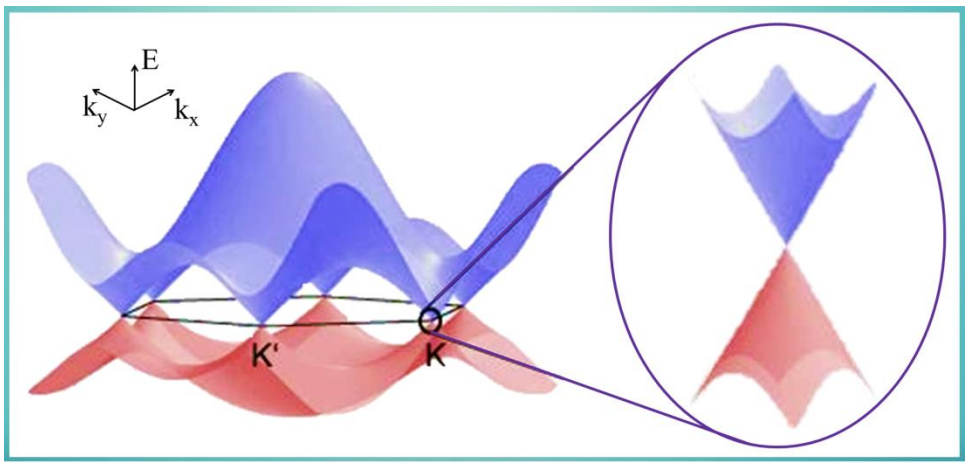

Figure 1.8 Electronic dispersion of graphene with zoomed view of the dispersion around the *K* point [35].

The Fermi level lies exactly at these points. Near this point, the graphene energy (*E(k)*) shows a linear dispersion relation (**relation (1.1)**), which results in massless excitons obeying the Dirac equation (better known as Dirac fermions) [36].

$$E(k) = \pm \hbar |k| v_F \qquad \textbf{(1.1)}$$

where $\hbar$ is the reduced Planck's constant, k is the quasi-particle momentum and $v_F$is the Fermi velocity (= 10^6 m s^{-1}) [35].

The electronic properties of graphene are highly affected on the number of layers **(Figure 1.9)**.Graphene bilayer has a parabolic spectrum (no Dirac points) around the Fermi energy, and with a very low band overlap of 0.16 meV, so it is often approximated as a zero-gap semi-conductor. However, the gap of the bilayer can be opened by applying an external electric field [37]. Graphene trilayer acts like a combination of graphene monolayer and bilayer, with the reappearance of the Dirac points [43]. With increasing number of layers (from 4 to <10), the electronic spectra become increasingly complicated with the appearance of several charge carriers. The conduction band and the valence band start to overlap, and the material shows semi-metallic behavior. The three- dimensional limit (graphite) is reached when the number of layers becomes 10 or more. Graphite shows semi-metallic behavior with a band overlap of ~ 41 meV [38].

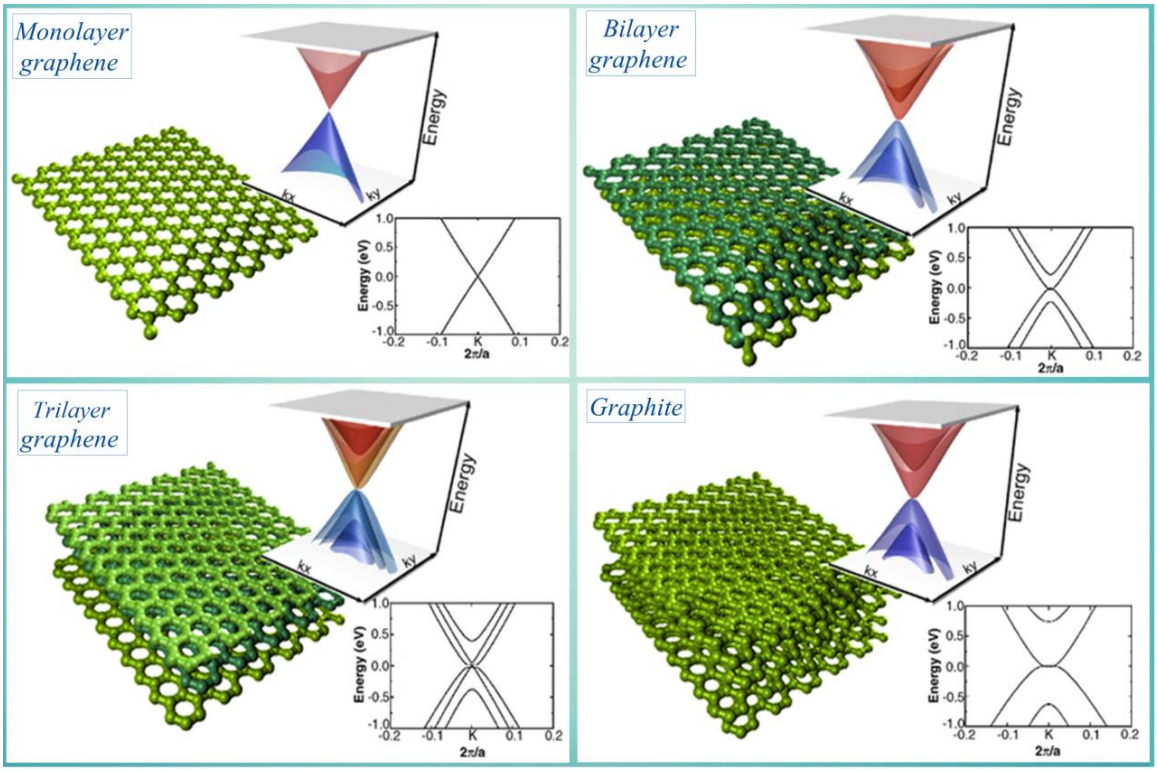

Figure 1.9 Low energy density functional theory three-dimensional band structures of monolayer, bilayer and trilayer graphene, and graphite [43].

A direct consequence of existence of massless charge carriers in graphene is its high room-temperature mobility (>2,00,000 cm^2 V^{-1} s^{-1} at electron densities of ~2 $\times 10^{11}$ cm^{-2} by suspending single layer graphene) [39]. Graphene also possess outstanding thermal properties and mechanical strength. It has thermal conductivity of ~5000 W m^{-1} K^{-1} at room temperature [40] and a Young's modulus of ~1.0 TPa[41]. In addition, graphene is also very light at 0.77 mg m^{-2}, often prompting researchers to say that a single sheet of graphene weighing under 1 g is sufficient to cover a whole football field [42].

In recent years, numerous methods have been established for synthesis of graphene. They can be broadly classifies into two approaches:

i. Top-down approach.

(a) *Mechanical exfoliation*. Graphene sheets of different thickness are peeled off/exfoliated from graphitic materials like highly ordered pyrolytic graphite (HOPG) by different routes like using a scotch tape [6], ultrasonication [43], electric field [44], atomic force microscopy (AFM) or scanning tunneling microscopy (STM) tips [45], etc.

(b) *Chemical exfoliation.* Graphite is treated with mixtures of sulfuric and nitric acids to form a graphite intercalated compound (GIC) so as to reduce the interlayer van der Waals forces, followed by rapid evaporation of the intercalants [46].

(c) *Chemical synthesis*. Graphite is oxidized to graphene oxide, followed by chemical reduction (discussed in detail in section *1.2.2.3.1*).

ii. Bottom-up approach.

(a) *Solvothermal synthesis*. Ethanol and sodium are reacted in 1:1 ratio in a closed vessel. An intermediate solid is formed that is then pyrolized to give a fused array of graphene sheets, which can be detached by sonication [47].

(b) *CVD*. A substrate is exposed to precursors (i.e., molecules that are converted to gaseous state by heating), which react and decompose on its surface to produce graphene [48].

(c) *Epitaxial growth*. Epitaxial crystalline graphene is grown on a single crystalline silicon carbide (SiC) surface. Graphitization occurs by sublimation of silicon at high temperature (1200 °C- 1800 °C) and high vacuum. At such high temperatures, silicon atoms desorb while carbon atoms remain behind to form graphitic layers [49].

Pristine graphene is relatively chemically inert. However, they can be made chemically labile by chemical functionalization of the graphene [50]. It is noteworthy that graphene is flat, thus chemical functionalization is not facilitated by curved surface induced strain in sp^2 bonds like it happens in case of fullerenes and CNTs. Functionalization of graphene sheets can be achieved in two different ways:

(i) *Covalent functionalization.*It involves the disruption of sp^2 bonds, and can be achieved using a wide variety of reactions, such as:

(i.i) treating graphene with atomic hydrogen to form "*graphane*" (a fully hydrogenated graphene sheet) [51],

(i.ii) treating graphene with halogen atoms such as fluorine [52], and

(i.iii) chemical oxidation of graphene, etc.

(ii) *Non-covalent functionalization*. Small molecules containing aromatic rings bind to graphene by van der Waals forces without forming any covalent bond. It also doesn't disrupt the sp^2 bonding network, but is generally weaker than covalent attachment.

1.2.2.3.1 Graphene oxide (GO)

Production of single layer graphene is very expensive and relatively difficult, thus efforts are being devoted to find cheap ways of making graphene, in large quantities, by using graphene derivatives or related materials. GO is one such material which is the oxidized form of graphite, and acts as a precursor to graphene.Although, technically, GO is single-layered like graphene **(Figure 1.10 (a)** and **(b))**, their chemical and physical properties are drastically different. As described by the Lerf–Klinowski model, GO is rich in oxygen-containing functional, i.e., they contain epoxy and hydroxyl groups on the basal plane and carbonyl and carboxyl groups at the edge planes [53], so they can be easily dispersed in a number of solvents. However, oxidation of graphite disrupts the sp^2 network, with the structure of GO having both disordered sp^3-bonded carbon and ordered sp^2-bonded carbon. This disruption renders GO insulating in nature [54].

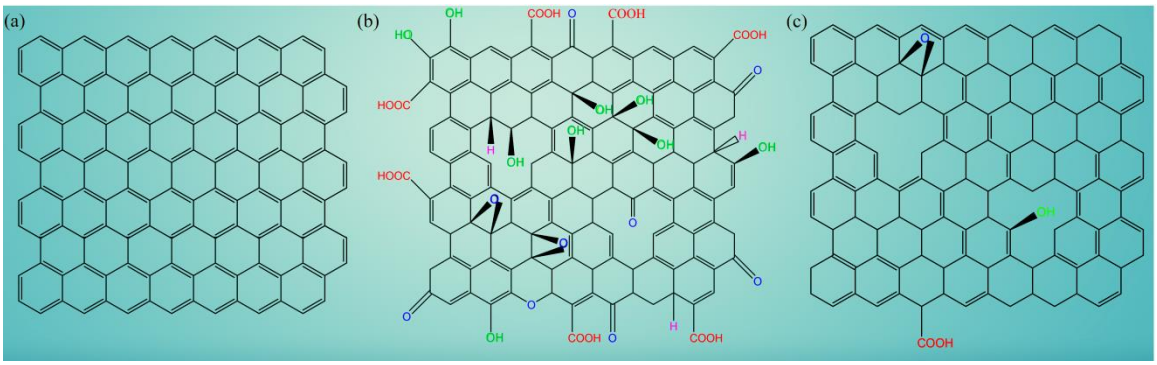

Figure 1.10 Structures of **(a)** graphene, **(b)** GO and **(c)** rGO.

The first documented synthesis of GO is credited to B. C. Brodie [55]. In the year 1859, with the intent of finding the atomic weight of graphite, he heated it with a mixture of potassium chloride ($KClO_3$) and fuming nitric acid (HNO_3), and observed that graphite disintegrated with the evolution of gas. When the disintegrated material was washed and re-oxidized for four or five times, it gradually underwent a change in appearance, until the material was completely converted into a light yellow colored substance. This resulting substance obtained by him was a mixture of graphene and GO, which was soluble in water. Nowadays, GO can be prepared by the two principal methods described in the following section. These different methods typically use

concentrated sulfuric acid (H_2SO_4) in combination with other chemicals, which affect the composition of the oxygenated groups, and consequently determine the chemical profile of the GO thus synthesized.

(a) *Staudenmaier method*[56]: In 1898, Staudenmaier improvised the Brodie's method by incorporating two main changes: (a) adding H_2SO_4 to increase the acidity of the reaction mixture and (b) adding multiple aliquots of $KClO_3$ over the course of reaction. GO thus obtained was highly oxidized, with a C/O atomic ratio of 2.89:1. The whole reaction occurred in a single reaction vessel, so he was able to simplify the GO production process. Nonetheless, the major disadvantage of this method is that it generates the toxic chlorine dioxide gas (ClO_2) toxic gas which rapidly decomposes in air to produce explosions. Also, it is a time-consuming process with addition of $KClO_3$ typically lasting over a week.

(b) *Hummers Method* [57]. In 1958, Hummers and Offeman proposed an alternative method of producing GO accompanied by a drastic reduction in reaction time, from 10 to 2 days. They mixed graphite with concentrated H_2SO_4, sodium nitrate ($NaNO_3$) and potassium permanganate ($KMnO_4$) to obtain a brownish grey paste. The suspension was then diluted with water and hydrogen peroxide (H_2O_2) was added to reduce the residual permanganate and manganese dioxide (MnO_2) to soluble manganese sulfate ($MnSO_4$), which was filtered-off. The resulting GO had a C/O ratio between 2.1:1 to 2.9:1.

1.2.2.3.2 Reduced graphene oxide (rGO)

Reduction of GO is essential to recover the honeycomb hexagonal lattice structure of graphene and restore its electrical conductivity **(Figure 1.10 (c))**. There are main two strategies for obtaining rGO.

(a) *Chemical reduction*. Hydrazine (N_2H_4) is the most common reagent used to obtain rGO sheets [58]. However, hydrazine is highly toxic and it introduces extra nitrogen functional groups during the reduction reaction, which sometimes restricts its applications. Another common reagent is sodium borohydride ($NaBH_4$) [59]. It is more effective than hydrazine in reducing carbonyl groups, but not highly effective in reducing epoxy and carboxylic acid groups.

The electrical conductivity of rGO is generally enhanced during the chemical reduction reaction, but the quality of the resulting product is relatively poorer than that of pristine graphene as it is difficult to completely recover from the defects within the sp^2 hexagonal lattice, caused by the chemical treatments (first oxidation, then reduction).

(b) *Thermal annealing*. GO is directly heated in a furnace to remove the oxygenated groups. At high temperatures (~1000 °C), carbon monoxide (CO) or carbon dioxide (CO_2) gases are rapidly evolved. The rapid heating also generates high pressure (~130 MPa), which is

sufficient to isolate the graphene sheets. However, release of the gases also causes structural and topological damage, which cause upto 30% mass loss [60].

1.2.2.3.3 Reduced graphene oxide aerogel

Interestingly, reduction of GO into rGO causes agglomeration of graphene sheets due to π-π interactions between them [61]. This is a grave concern for its applications. In order to realize the full potential of graphene, it is of utmost importance to address this issue. One method is to convert the two-dimensional graphene into three-dimensional aerogel **(Figure 1.11)**. Invented in 1931 by S. S. Kistler[62], aerogels are highly porous nanomaterials (90-99% porosity) characterized by ultra-low density (0.16 mg cm^{-3} for carbon aerogels [63]), high surface area, large pore volumes and low thermal conductivity [64].

Figure 1.11 Carbon aerogel balancing on the blade of grass.

Reduced graphene oxide aerogel (rGOA) is an important class of carbon aerogels. GO is the most popular precursor to prepare rGOA. Its key advantages include its high dispersion in aqueous medium and the presence of oxygenated groups that can react covalently with other compounds to produce new materials. The common routes for producing rGOA can be broadly divided into two categories: self-assembly method and template-directed method [65,66].

(a) *Self-assembly method.*

In a stable GO suspension, there is a balance between two forces: electrostatic repulsion due the functional groups present on GO, and van der Waals attraction due to the basal planes of GO. This balance ensures their proper dispersion in aqueous medium. But when this balance is lost, gelation of the GO suspension starts. The GO sheets cross-link with each other to form a wet (or hydro-) gel, which is then freeze- or supercritical fluid dried. The drying process removes the solvent from the wet gel and replaces it with air to give the aerogel [67]. Self-assembly can be induced by a number of agents like:

(i) *Hydrothermal reduction induced self-assembly of GO*[68].

(ii) *Chemical reduction induced self-assembly*. Mild reducing agents like hydrazine, L-ascorbic acid, sodium ascorbate, $NaBH_4$ and sodium sulfide (Na_2S) are employed to reduce GO [69].

(iii) *Cross-linking agent induced self-assembly.* Different cross-linking molecules facilitate the self-assembly of rGOA, e.g.,

- multivalent ions (e.g., calcium (II) ions (Ca^{2+}), magnesium (II) ions, (Mg^{2+}), chromium (III) ions (Cr^{3+})) [70],
- layered double hydroxides (LDHs) [71] ,
- biomolecules (e.g., deoxyribonucleic acid (DNA), polyamines) [72] ,
- polymers (e.g., poly(vinyl alcohol) (PVA), polyethylenimine (PEI)) [73], and
- monomers (e.g., aniline, pyrrole) [74], etc.

(iv) *Organic sol-gel chemistry driven self-assembly.* Sol-gel chemistry has also been employed to cross-link GO sheets *via* polymerization of resorcinol (R) and formaldehyde (F) [75]. With sodium carbonate (Na_2CO_3) as a catalyst, the polymerization reaction creates strong covalent bonds between the sheets. Due to this, rGOA produced by this method show better electrical conductivity than those produced by physical cross-linking.

(b) *Template-directed method.*

It is a very useful method for obtaining porous aerogels since the random cross-linking of graphene sheets is prevented by the template, while favoring controllable microstructure formation. Nickel (or copper) foam-directed CVD approach is quite common for growing free-standing graphene aerogels [76,77].

1.2.3 Other forms of carbon

1.2.3.1 Amorphous carbon

Carbon materials without any long-range crystalline order are grouped as amorphous carbon. The materials can be a mix of sp^3, sp^2 and even sp^1 hybridized carbon atoms, with a high concentration of dangling bonds. The ratio of the hybridized atoms determines the short-range order in amorphous carbon [78]. The carbon network shows a lot of deviations in both bond distances and bond angles. Different forms of amorphous carbon include activated charcoal, carbon black, lamp black, etc.

Carbon black (CB)

CB is a particulate form of carbon, comprising spherical particles with diameter ranging from 10-100 nm and surface area in the range of 25-1500 $m^2\ g^{-1}$. It resembles graphite more than it does diamond, but the hexagonal layers are farther apart and have no vertical orientation. Three to four such hexagonal layers join in bundles and form the *primary particles* of CB **(Figure 1.12)**. These particles then fuse together in clusters to form the characteristic units of CB, called

the *aggregates*. The actual structure of CB is determined by the number of primary particles present per aggregate. And based on this, CB can be categorized into "*high-structure"* CB (aggregates are composed of high number of primary particles, with considerable branching and chaining) and "*low-structure"* CB (aggregates are composed of low number of primary particles) [79].

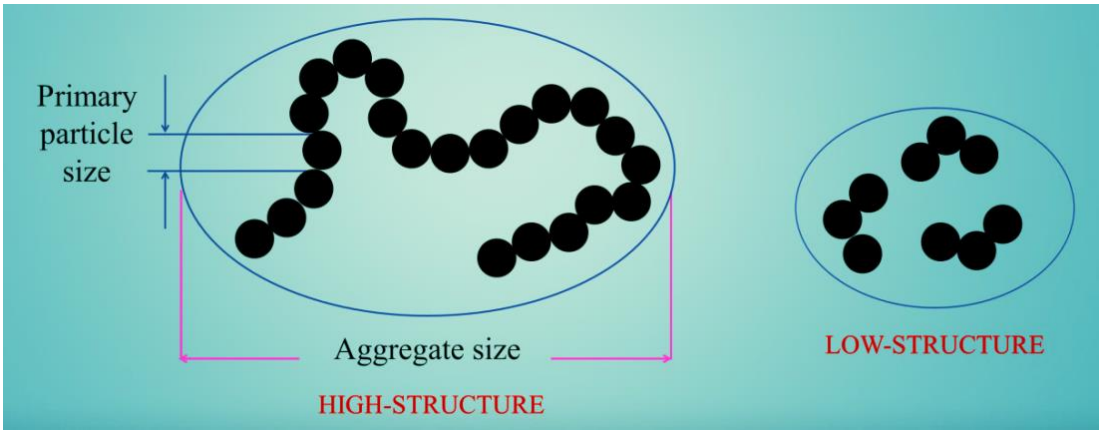

Figure 1.12 Structure of CB.

The structure and specific surface area of CB are considered as its two most important features. The surface area of CB is inversely proportional to the diameter of the particles, while the structure, particularly the graphitic character of the first atomic layer, exerts a strong influence on its electrical conductivity [80].

1.2.3.2 Carbon dots (CDs)

CDs are the newest member of the carbon nanoparticle family with size less than 10 nm [81]. They were serendipitously discovered in 2004 by Xu and co-workers during the purification of SWCNTs [82]. The most significant property of CDs is their strong photoluminescence (PL), comparable to that of current inorganic semi-conductor quantum dots (SQDs), but with the additional advantage of being negligibly toxic. It would be interesting here to note that in literature, various terms like carbon nanodots (CNDs), carbon quantum dots (CQDs) and graphene quantum dots (GQDs) are frequently used for fluorescent carbon nanoparticles (FCNs). According to Cayuela*et al*., CNDs (are also referred to as carbon nanoclusters, polymer dots or CDs) can be described as amorphous nanodots which lack quantum confinement, and consist mainly of sp^3carbon atoms in a disordered structural core. On the other hand, nanoparticles with quantum confinement and crystalline structure are termed as CQDs, wherein the crystalline core is composed of a mixture of sp^2 and sp^3 hybridized carbons. GQDs are completely different in the sense that they are essentially a disk of π-conjugated single graphene sheet with a diameter of 2–20 nm **(Figure 1.13)**[83]. Although this is one way of classifying FCNs (also reinforced by Zhu *et al.*[84]), there are so many structures with varying degrees of crystallinity and different

morphologies that have been reported to be synthesized that the name and classification of CDs is still open question. One popular view is that the CDs are quasi-spherical nanoparticles with a diverse combination of aromatic (sp^2 hybridized graphene-type islands rich in π-electrons) and aliphatic (sp^3 hybridized diamond-type inclusions) regions with different surface functional groups [85]. In this thesis, we will use the term CDs for both CQDs and CNDs from hereon.

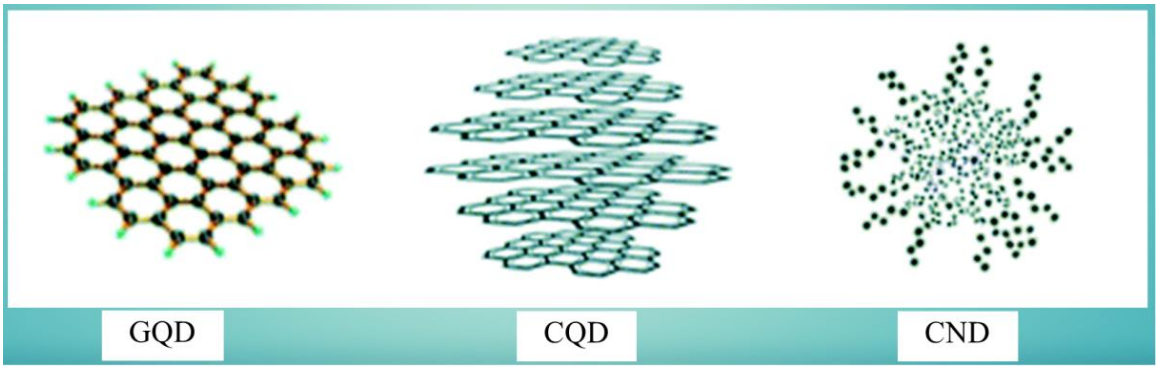

Figure 1.13 Structures of different FCNs: GQDs, CQDs and CNDs [83].

The most fascinating feature of these FCNs, both from fundamental and application point of view, is their excitation-dependent PL. Currently, this property is mainly attributed to either optical selection of differently sized nanoparticles (i.e. quantum size effect) or the presence of different emissive traps on the surface of CDs.

- *Quantum size effect*. PL properties vary sensitively with the size of CQDs. The emission is mainly caused by fragments of quantum-sized graphite structure [86]. As the size of the fragment increases, the highest occupied molecular orbital (HOMO) – lowest unoccupied molecular orbital (LUMO) gap gradually decreases.
- *Surface states as PL centers*. Functional groups have different energy levels, which manifests as a series of emissive traps. When CD is excited with the light of a particular wavelength, a particular surface state emissive trap dominates the emission **(Figure 1.14 (a))**. The surface state is not an isolated chemical group but rather the combination of the carbon backbone and connected chemical groups. A higher degree of surface oxidation causes more surface defects, which can cause a red-shifted emission.

Another interesting phenomenon associated with CDs is *up-converted PL*. This effect is also referred to as *multi-photon PL*, since it occurs as a result of a multi-photon process. In this process, two or more photons (usually near-infrared with lower energy) are absorbed resulting in the emission of a single photon with higher energy **(Figure 1.14 (b))** [87].

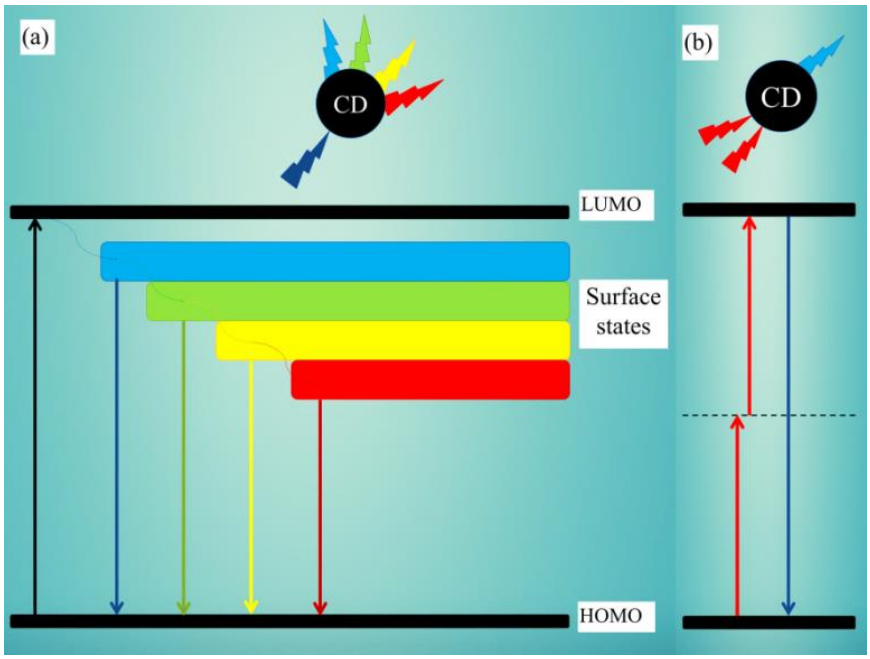

Figure 1.14 Electronic states in CDs. **(a)** Surface states as PL centers in down-conversion process and **(b)** multi-photon excitation in up-conversion process.

The methods for synthesizing FCNs are generally divided into two groups based on their approaches: top-down and bottom-up. In the top-down approach, materials like graphite, CNTs, GO, carbon fibers, etc. are used as carbon sources, thus the nanoparticles formed by this route are termed as GQDs or CQDs. Meanwhile, in the bottom-up approach, small organic molecules are used as carbon sources, and are denoted as CNDs (or CDs). Saccharides, citric acid and amino acids are some of the popular carbon sources. Eggs [88], pomelo peel [89] and potato starch [90] have also been carbonized to produce CDs through synthetic methods such as hydrothermal reaction [91], ultrasonic [92] and microwave irradiation [93].

1.3 Carbon based nanocomposites

Nanocomposites are defined as the combination of two or more phases of materials in which at least one constituent has one dimension less than 100 nm. Typically, a nanocomposite is a matrix-filler combination, where the nano-sized fillers are surrounded by a matrix. Nanoparticles (as fillers) at very low volume fractions can influence the properties of the nanocomposites. Due to their small size, the fillers generate a large number of contact points at the filler-matrix interfaces. In addition, high surface area of the fillers also contributes to synergistic improvements in the properties of the nanocomposite, where the final properties are far more superior to those of the individual components. Since the filler volume fraction is quite low, it allows the nanocomposites to retain the macroscopic homogeneity as well [94].

There are different categories of nanocomposites depending on the type and nature of the matrices and fillers. In this thesis, we will deal with two-types of nanocomposites: (a) *polymer matrix nanocomposite* and (b) *metal oxide matrix nanocomposites*.

(a) Polymer nanocomposites: Polyaniline matrix

Polymer nanocomposites consist of nanoparticles surrounded by an organic polymeric matrix. Recently, *hybrid electrically conducting nanocomposites* - the combination of conducting nanoparticles and intrinsically conducting polymers (ICPs) - has emerged as a new field of interest [95]. Leading its way are carbon based nanomaterials (like CNTs, graphene, etc.) as fillers, courtesy of their lucrative properties like high electrical and thermal conductivities, high surface area, high strength and stiffness along with flexibility.

The pre-requisite for an ICP is the presence of either a conjugated structure with alternating single and double bonds or conjugated segments coupled with atoms (e.g., N, S, etc.) providing p-orbitals for a continuous orbital overlap. These polymers do not have any intrinsic charge carriers, thus the necessary charge carriers required for insulator-to-metal transition are provided by either oxidation of the polymer chain with electron acceptors (*p-doping*) or by reduction with electron donors (*n-doping*). The doping process introduces charged defects like polarons and bipolarons, which act as charge carriers.

Among the ICPs, polyaniline (PAni) has become technologically very important one due to its processability, availability of inexpensive monomer and high yield of polymerization. PAni exists in three oxidized states: (a) fully reduced leucoemeraldine base, (b) conducting emeraldine base with equal number of reduced and oxidized units, and (c) fully oxidized pernigraniline form. All these forms can be inter-converted by protonation and de-protonation reactions **(Figure 1.15)** [96].

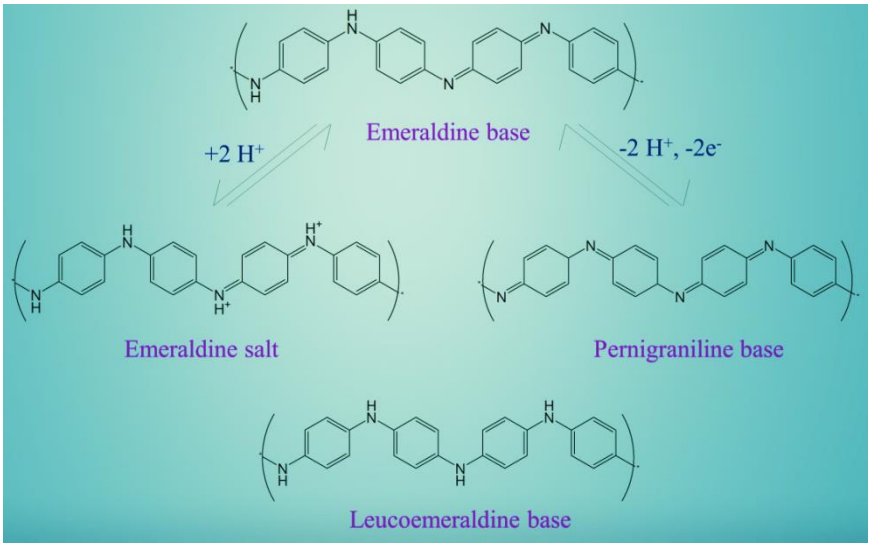

Figure 1.15 Different oxidation states of PAni.

PAni is a *p-type* semi-conductor [97]. Its conductive nature is one of its most fascinating properties. Its exact conduction mechanism is not clear, but there are a few theories. When PAni (emeraldine base) is doped, say with a protonic acid, a polaron (spin = 1/2) is formed through the successive formation of a bipositive species and a bipolaron (spin = 0) **(Figure 1.16)**. The polaron structure exists as a cation radical on imine nitrogen atom, and acts as a hole (charge carrier). The electron from the adjacent neutral nitrogen can jump to that hole. During the process, this hole becomes neutral and a second hole is created on the adjacent nitrogen. The charge carriers propagate in this manner, leading to an electrical conduction along the chain.

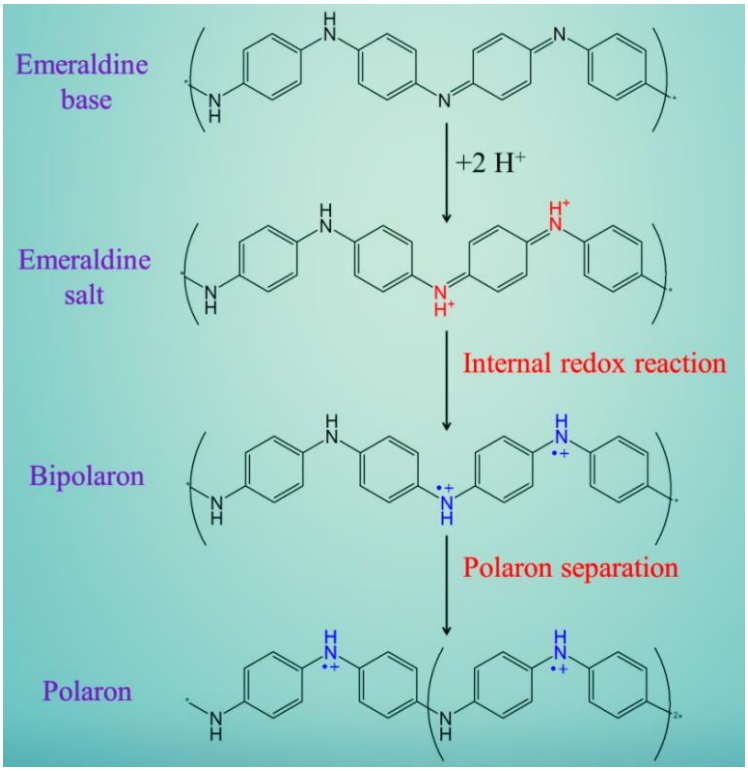

Figure 1.16 Formation of polarons *via* bipolarons.

There is another model to explain the conductivity of PAni - the band model. According to it, when PAni is doped, an electron is removed from the polymer producing a free radical and a positive charge [98]. The introduction of charges causes a structural distortion of the polymer around the charge. Thus, polaron can be defined as a charge (radical cation) in the extended lattice that is stabilized by a local distortion of the lattice. Upon further oxidation, the free radical of the polaron is removed and a bipolaron is created. A bipolaron is formed either by coupling of two pre-existing polarons, or by addition of charge to a pre-existing polaron. At higher doping levels, polarons are gradually replaced by bipolarons, and they eventually form continuous bipolaron bands in the forbidden gap **(Figure 1.17)**.

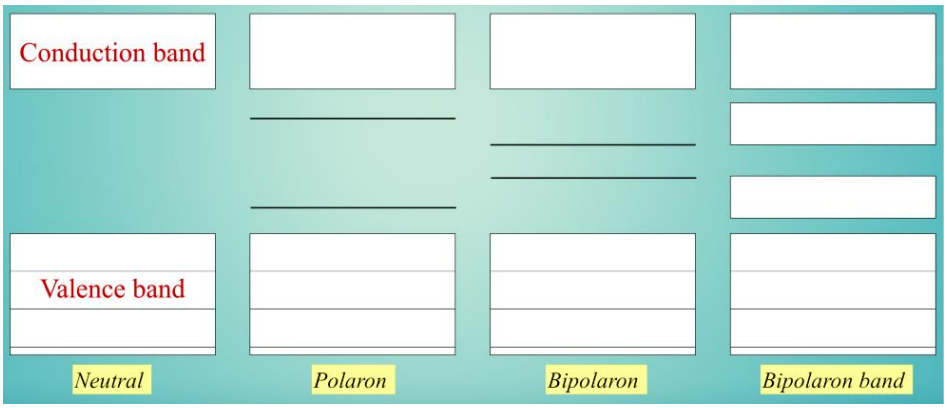

Figure 1.17 Schematic representation of energy levels of PAni.

(b) Metal nanocomposites

(i) *Noble metal nanoparticles*

Noble metal nanoparticles like gold (Au), silver (Ag) and platinum (Pt) are a unique class of functional materials whose physical and chemical properties are closely governed by their size and shape. The large surface-to-volume ratios of these nanoparticles in comparison to bulk have made them popular in a large number of areas, including catalysis, electrochemical and electrical applications. However, scarcity and high cost of noble metals necessitates their integration with other materials so as to minimize their consumption. So far, nanocomposites have been successfully synthesized with polymers, biomaterials and carbon materials incorporated with noble metal nanoparticles [99]. Among them, graphene based metal nanocomposites are particularly interesting since, in addition to the inherent properties of graphene, they can also act as high surface area support for the metal nanoparticles [100].

(ii) *Metal oxide nanoparticles*

Titanium dioxide (TiO_2) is the naturally occurring form of titanium, ubiquitous and robust. It occurs as three major crystal structures: rutile (tetragonal structure), anatase (tetragonal structure) and brookite (rhombohedral structure). TiO_2 is an *n*-type wide band-gap semi-conductor (band-gap energy = 3.2 eV), and is most utilized as a photo-catalytic agent. Under photo-excitation, electron hole pairs (charge carriers) are generated in TiO_2. It is the main driving force underlying its catalytic behavior. However, these charge carriers have the tendency to recombine and lower the catalytic activity. To overcome this drawback, noble metal/TiO_2 nanocomposites are often used, which show better charge separation between the charge carriers accumulating on its surface [101]. Recently, *noble metal/metal oxide nanocomposites* haveemerged as a special category of nanocomposites that are especially suited for numerous catalytic and solar applications [102]. Examples of such nanocomposites include Au/TiO_2, Ag/zinc oxide (ZnO), Pt/TiO_2, etc. In addition to preventing the recombination effect by forming

Schottky barriers, coupling of metal oxides with noble metals also widen their light absorption range.

1.4 Applications of carbon based nanomaterials

1.4.1 Sensors

Functional carbon nanomaterials like CNTs, CDs as well as their nanocomposites display superior mechanical, electrical and optical properties. These properties can be easily tapped into to develop highly sensitive and selective sensors. Depending on the material used, sensing effects may involve physical, chemical, electrical or optical changes, or a combination of effects between them.

1.4.1.1 Gas sensors

Gas sensors, or chemical sensors, are of tremendous interest because of their ability to detect gases and volatile organic compounds (VOCs), which is critical for human health and environment safety. Any good sensing system must comply with the following criteria:

- high sensitivity and selectivity,
- fast response and recovery time,
- room temperature operation and temperature independence, and
- good stability.

CNTs have been on the forefront of gas sensors, ever since their discovery. There are two particular properties that make CNTs extremely favorable as gas sensors. First, as one-dimensional materials, their ‘quantum nature’ makes their electrical conductance highly sensitive to minute external modulations. [103]. Second, the high active surface area and hollow structure is highly advantageous for the molecules to get adsorbed to [104]. When CNTs are exposed to vapors, the gas molecules get adsorbed on its surface and change its electrical resistance. This effect forms the basis for a resistance-based gas detecting system [105].

J. Kong *et al.* have successfully reported chemical sensors based on semi-conducting individual SWCNTs for detection of nitrogen dioxide (NO_2) and ammonia (NH_3) gases based on the above mechanism [106]. The same group also fabricated a palladium coated SWCNT sensing platform for detecting perturbations in electrical conductivity on exposure to molecular hydrogen gas (H_2) [107]. There are numerous reports of similar sensing platforms using either pristine CNTs or metal decorated CNTs or CNT/polymer nanocomposites for detection of gases like oxygen (O_2; SWCNT) [108], carbon monoxide (CO; Au decorated SWCNT) [109], NH_3 (MWCNT/PAni) [110], methanol (SWCNT/Nafion) [111], etc. Decorating CNTs with other materials boost the analyte sensitivity.

In the recent years, the field of graphene-based sensors is also catching-up. The electrical response of graphene to different gases is comparable to that of CNTs [112,113]. However, there are certain discrepancies in the reported results. For instance, Novoselov and co-workers [114], and Johnson and co-workers [115] observed decreased resistance of graphene based sensing devices on exposure to water vapor, while Ruoff and co-workers observed the exact opposite effect [116]. Ultimately, these inconsistencies were accredited to the experimental set-up and presence of contaminants. It is now believed that the intrinsic sensitivity of graphene-based sensors is actually fairly low, but can be increased during the device fabrication, *via* contaminants. The contaminants can be considered as dopants similar to metal or polymer doping in CNTs [117].

1.4.1.2 Fluorescence based sensors

Fluorescence based sensing requires the presence of a fluorescent material (i.e., a fluorophore) whose PL intensity can undergo change in the presence of an analyte. Many such sensing platforms have been developed using organic dyes, quantum dots, and more recently, CDs. The sensing activity is primarily governed by either *photo-induced electron transfer (PET)* process [118], *fluorescence resonance energy transfer (FRET)* process [119] or *inner filter effect (IFE)* [120].

CDs can display colorful PL and has high photo-stability, hence they can serve as sensors for a broad range of analytes. The most-reported analytes comes from the group of metal ions. Examples of cations detected using CDs include copper (II) ions (Cu^{2+}) *via* IFE [121], mercury (II) ions (Hg^{2+}) *via* electron or energy transfer process[89], ferric ions (Fe^{3+}) *via* non-radiative electron transfer process [91], chromium (VI) ions (Cr^{6+}) *via* IFE [122], lead (II) ions (Pb^{2+}) *via* non-radiative electron transfer process [123], etc. The field of anion detection is comparatively less developed in contrast to cations. Nonetheless, anions such as iodide ions (I^-) [124], hypochlorite ions (ClO^-) [125], superoxide anions ($O_2^{\bullet-}$) [126], etc. have been probed using CDs. Low-molecular weight thiols such as glutathione [127] and cysteine [128], glucose [129], hydrogen peroxide (H_2O_2) [130], and nitroaromatic compounds (NACs) like picric acid [131] have also be detected using CDs.

1.4.2 Dye sensitized solar cells

The conversion of sunlight (photo-) to electricity (-voltaic) is known as the *photovoltaic effect*. Demonstrated for the first time in the year 1839 by A. -E. Becquerel, the photovoltaic effect is the foundation of all solar cells including dye sensitized solar cell (DSSC) [132]. DSSC is a third generation solar cell, co-invented by B. O'Regan and M. Grätzel in 1991 [133]. These cells are very popular for their cost-effectiveness and easy fabrication technique. So far, the

highest photo-conversion efficiency obtained from a DSSC is 14.3% [134]. A DSSC is fundamentally composed of three main components, described briefly in the next section.

(i) *Photo-anode.* A wide band-gap semi-conductor like nano-crystalline mesoporous TiO_2 adsorbed with sensitizer dye molecules acts as the photo-anode. The dye molecules absorb sunlight and generate photo-electrons. [135].

(ii) *Electrolyte*. The electrolyte is responsible for shuttling the charge carriers between electrodes inside the cell. It continuously regenerates itself as well as the dye during DSSC operation. A redox couple, the solvent and additives comprise the three main constituents of an electrolyte [136].

(iii) *Counter electrode*. The counter electrode is responsible for catalyzing the reduction of I_3^- ions. Pt is mostly used to fabricate DSSCs demonstrating high efficiencies due to high electrical conductivity, low charge transfer resistance, good catalytic activity towards triiodide reduction, corrosion resistance and high reflecting properties [137]. However, higher cost and less abundance necessitates the search for its replacement by low-cost materials like carbon [138], metal alloys [139], polymers [140], composites, etc.

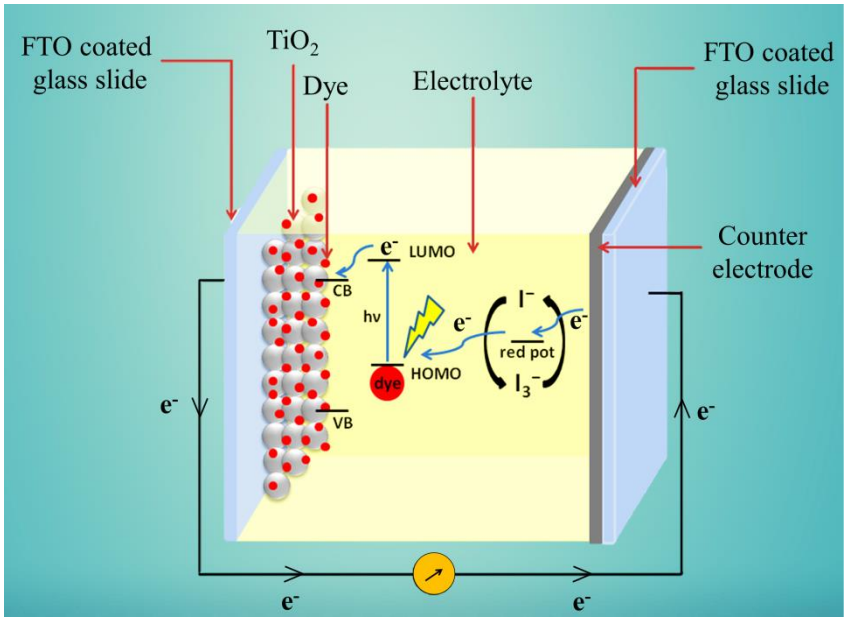

Figure 1.18 Different components of a DSSC with its working mechanism.

The DSSC is fabricated by placing the electrolyte between the photo-anode and the counter electrode using a spacer. The dye molecules absorb sunlight and generate photo-electrons (get oxidized in the process), which are then injected into the conduction band of TiO_2. They then diffuse through the external circuit and reach the counter electrode. At the electrode, these electrons reduce I_3^- to I^-. The oxidation of I^- back to I_3^- promotes regeneration of the oxidized dye **(Figure 1.18)**.

1.4.3 Supercapacitors

The changing global landscape has highlighted the urgency of developing efficient energy storage devices. *Batteries*, with high energy density, have traditionally fulfilled the role of storing energy (including light-weight and portable devices). Batteries store charge *via* redox reactions at the electrodes during charging and discharging. For instance, in case of lithium ion batteries, the lithium ions migrate into the anode during charging and away from it during discharging **(Figure 1.19 (a))**. But flammable organic solvent based electrolyte can cause explosion in case of short-circuit, while low power density and short battery life due to swelling or dissolution of active materials during the faradaic reactions also raise concern [141]. To combat these issues, *supercapacitors* are now being explored. Supercapacitors are characterized by a high power density and long cycle lives with no short-circuit concerns. However, they have relatively lower energy density, i.e., while a battery can store more energy per unit volume (or mass) but cannot release it quickly, a supercapacitor, on the other hand, can store relatively less energy but can discharge it very quickly to produce more power.

A conventional *capacitor* (also called an *electrostatic capacitor* or a *parallel plate capacitor*) consists of two conducting metal plates separated by an insulating dielectric. When an external voltage is applied, opposite charges get accumulated on the surfaces of the two plates **(Figure 1.19 (b))**. Since the charges cannot cross over, an electric field is generated which allows the device to store energy. A capacitor is characterized by a parameter called the *capacitance* (C), which represents its ability to store charge (q). The capacitance is mathematically given by **relation (1.2)**.

$$C = \frac{q}{V} = \frac{\epsilon_O \epsilon_r A}{d} \qquad \textbf{(1.2)}$$

where ε_o, ε_r, A and d represent permittivity of free space, relative permittivity of the dielectric medium, area of the electrode and distance between the plates respectively. Energy density and power density are two integral parameters of any energy storage device. The energy stored in a capacitor (E') is given by **relation (1.3)** while the power (P) can be determined by differentiating E' with respect to time required for discharge (t) **(relation (1.4))**.

$$E' = \frac{1}{2} C V^2 = \frac{q^2}{2C} \qquad \textbf{(1.3)}$$

$$P = \frac{\partial E'}{\partial t} \qquad \textbf{(1.4)}$$

Now, on the basis of their working mechanism, supercapacitors can be divided into three categories as described below.

(i) Electrochemical double layer capacitors (EDLCs). EDLCs contain two electrodes, an electrolyte and a separator, which allows the diffusion of ions through it but not of charges.

Governed by similar principles as a conventional capacitor, an EDLC also stores charges electrostatically (i.e., non-faradaically) *via* an electrochemical (or Helmholtz) double layer [142]. When voltage is applied, ions in the electrolyte solution migrate to the oppositely charged electrode and form a Helmholtz double-layer at each electrode **(Figure 1.19 (c))**. The electrodes are mostly porous, so an increased surface area along with the double-layers allows EDLCs to attain higher energy densities than conventional capacitors for similar sized devices. At the same time, the absence of any redox reaction at the electrodes speeds up the charge-discharge process since only absorption and desorption of ions occurs lifting the limitation of chemical reaction kinetics. Common EDLC electrode materials include graphene [143], activated carbon [144], carbon aerogels [145], CNTs [146], etc.

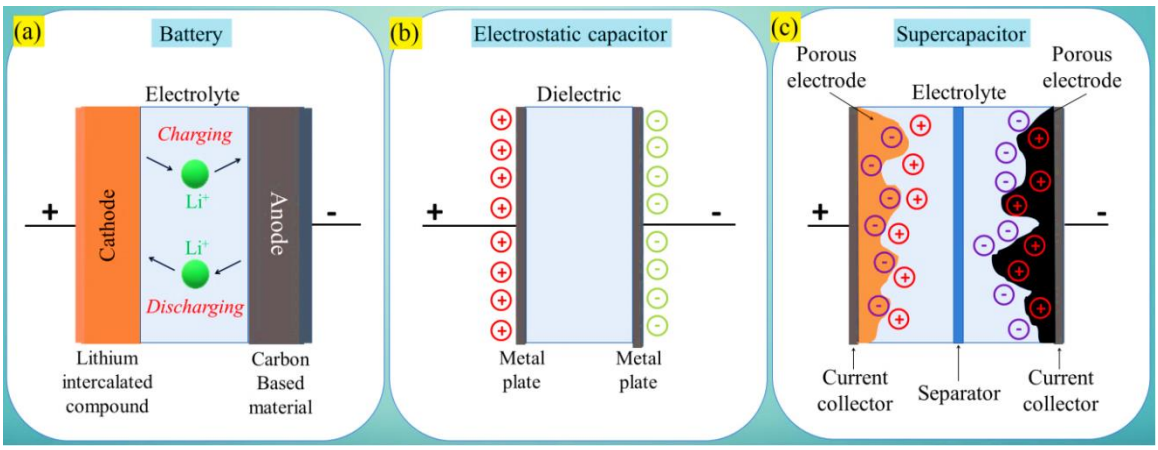

Figure 1.19 Charge storage mechanisms of **(a)** a battery, **(b)** a conventional capacitor and **(c)** an EDLC on application of external voltage.

(ii) Pseudo-capacitors. In contrast to EDLCs, a pseudo-capacitor uses active materials which can undergo fast and reversible faradaic reactions. In this respect, pseudo-capacitors are similar to batteries. Transition metal oxides such as MnO_2[147], ruthenium dioxide (RuO_2) [148] and nickel oxide (NiO) [149], ternary metal oxides and metal hydroxides such as nickel cobaltite ($NiCo_2O_4$)[150] and nickel hydroxide ($Ni(OH)_2$)[151], and ICPs like PAni [152] and polypyrrole[153] are examples of materials that possess pseudo-capacitance.

(iii) Hybrid supercapacitors. In an effort to increase the energy density of supercapacitors, hybrid supercapacitors have been designed that utilizes both faradaic and non-faradaic processes to store charge. Depending on the configuration, hybrid supercapacitors are either *composite hybrids*, *asymmetric hybrids* or *battery-type hybrids*[154,155]. A composite supercapacitor integrates a carbon based material with a pseudo-capacitive material in a single electrode [156], while an asymmetric supercapacitor uses two dissimilar electrodes: one showing EDLC behavior (negative electrode) and the other with pseudo-capacitive behavior (positive electrode) [157]. By employing two electrodes working in complementary potential ranges, the

thermodynamic breakdown of water (at 1.23 V) is avoided in such supercapacitors [158]. The inspiration for this design comes from **relation (1.3)**, where, by increasing the working voltage, a two-fold increase in the energy density can be achieved. Battery-type hybrid combines a supercapacitor electrode with a battery electrode [159].

1.4.4 Direct methanol fuel cells

Similar to supercapacitors, fuel cells also convert the chemical energy (of a fuel, mainly hydrocarbons, alcohols and hydrogen) into electricity. The advantages of a fuel cell are that the by-products of the reaction are environmental-friendly and among all the alternate energy storage devices, fuel cells provide the highest energy densities **(Figure 1.20)** [160]. There are no charge-discharge cycles involved, the cell will function as long as the fuel is available.

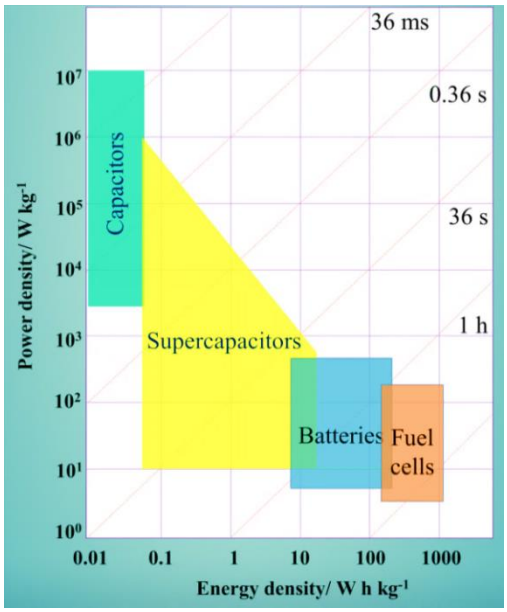

Figure 1.20 Ragone plot of different alternate energy storage devices.

Depending on the type of fuel used, fuel cells can be divided into different categories, one of which is the DMFC that uses methanol (CH_3OH). A DMFC consists of an anode, a cathode and an electrolyte. Methanol oxidation reaction (MOR) occurs at the anode and the reaction of methanol with water produces carbon dioxide (CO_2), along with protons (H^+) and electrons (e^-) **(relation (1.5))**. Meanwhile, the cathode produces water (H_2O) *via* reaction of oxygen (O_2) with protons and electrons produced at the anode **(relation (1.6)) (Figure 1.21)**. The overall process is exothermic.

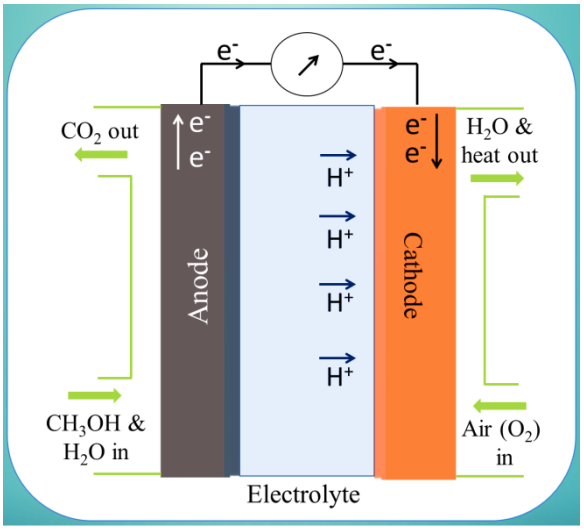

Figure 1.21 Working principle of a DMFC.

$$Anode: CH_3OH + H_2O \rightarrow CO_2 + 6H^+ + 6e^- \quad \textbf{(1.5)}$$

$$Cathode: {}^3/_2\, O_2 + 6H^+ + 6e^- \rightarrow 3H_2O \quad \textbf{(1.6)}$$

In reality though, MOR is not so simple but requires a highly effective catalyst to drive the reaction through a series of steps. Since the anode is an integral part of a DMFC, a major thrust area in fuel cell research is to design novel anode catalysts. Noble metals like Pt [100] and their bimetallic alloys like PtRu[161] are popular candidates for electro-oxidizing methanol. However, high cost of Pt has led to the search for other alternative approaches [162], like (a) using carbon nanomaterials as catalyst supports to prepare a uniformly dispersed supported catalyst [163], and (b) exploration of MOR using photo-catalysts like TiO_2[164] or a combination of both a photo-catalyst and an electro-catalyst with low noble metal content like Pt/TiO_2[165].

1.5 Objectives

Carbon based materials such as CNTs, graphene, carbon black and CDs have been extensively studied over the last few years due to their outstanding properties. A small amount of these materials, when added in a nanocomposite, can make significant improvements to their properties. Researchers are devoting their efforts to utilize these nanomaterials for numerous applications. For instance, CNTs are highly conducting and their dimensionality makes them a very good candidate for gas sensors. CB and graphene based aerogels have high porosity and large active surface areas, and these features make them ideal for use as electrodes in DSSCs and supercapacitors. CDs, in the other hand, have unique optical properties including up- and down-

conversion fluorescence, and these properties can be exploited as photo-catalysts, photo-anodes and sensors. Keeping these possibilities in mind, the objectives of this doctoral thesis are:

i. Synthesis of different types of carbon based nanomaterials:
   (a) MWCNT/PAni nanotube (MWCNT/PAniNT),
   (b) CB/PAniNT,
   (c) reduced graphene oxide aerogels (rGOA) functionalized (separately) with silver nanorods (AgNRs) and PAniNT, and
   (d) different colored CDs, as well as nanocomposite of blue-emitting CDs with TiO_2 and Pt ($Pt/CD/TiO_2$).

ii. Characterization of the prepared carbon based nanomaterials using different analytical tools.

iii. Applications of these materials in
   (a) methanol gas sensor (MWCNT/PAniNT),
   (b) DSSCs as counter electrode (CB/PAniNT) and co-sensitizers (green-emitting CDs),
   (c) asymmetric supercapacitor (rGOAs),
   (d) MOR ($Pt/CD/TiO_2$), and
   (e) picric acid sensor (blue-emitting CDs).

1.6 Plan of research

To realize these objectives, the following methodologies will be employed.

1.6.1 Synthesis of carbon based nanomaterials

The synthesis procedures will include:

(a) *in-situ* chemical oxidation polymerization of PAniNT in the presence of MWCNTs and CB particles to obtain MWCNT/PAniNT and CB/PAniNT nanocomposites respectively,

(b) a self-assembly driven sol-gel technique to prepare rGOA functionalized separately with AgNRs and PAniNT,

(c) hydro- or solvothermal synthesis of CDs from two different carbon sources (citric acid and gallic acid) under different reaction conditions. Hydrothermal route will be further employed to prepare CD/TiO_2 nanocomposite followed by chemical reduction of chloroplatinic acid to decorate them with Pt nanoparticles.

1.6.2 Characterization of the nanomaterials

The synthesized nanomaterials will be characterized using different analytical tools such as Fourier transform infra-red (FTIR) spectroscopy, X-ray photoelectron (XPS) spectroscopy, X-

ray diffraction (XRD), Raman spectroscopy, UV-visible spectrophotometer, fluorescence spectrophotometer, scanning electron microscopy (SEM), TEM and energy dispersive X-ray (EDX) spectrometry, etc.

1.6.3 Electrochemical tests of the nanomaterial electrodes and devices

Electrodes will be fabricated using spin-coating or doctor-blade technique and their electrochemical properties will be evaluated using cyclic voltammetry (CV), current density-voltage(*J*-*V*) characteristic plots, electrochemical impedance spectroscopy (EIS), galvanostatic charge-discharge (GCD) and chronoamperometry.

1.6.4 Application of the nanomaterials

(a) MWCNT/PAniNT nanocomposite will be shaped into a pallet and exposed to methanol vapors. The ensuing change in resistance will be recorded to assess their sensing behavior.

(b) DSSCs will be fabricated with N719 dye sensitized TiO_2 as photo-anode and CB/PAniNT nanocomposite as counter electrode with I^-/I_3^- redox couple based electrolyte. The catalytic activity of the nanocomposite for triiodide reduction and the performance of the devices under 1 Sun illumination will be investigated, and compared with that of Pt counter electrode.

(c) Flexible asymmetric supercapacitors will be fabricated with AgNR and PAniNT functionalized rGOA as anode and cathode, and their capacitive behavior will be examined.

(d) The photo-electrocatalytic activity of Pt nanoparticle supported on CD sensitized TiO_2 for MOR will be investigated.

(e) Solar cells with N719 dye and green-emitting CDs co-sensitized TiO_2 photo-anode, Pt counter electrode and I^-/I_3^- redox couple based electrolyte will be devised, and the effect of CDs as co-sensitizers will be studied.

(f) Blue-emitting CDs derived from gallic acid as carbon source will be applied as sensing element for detecting picric acid. Decrease in fluorescence intensity on interaction of CDs with the analyte will be used as a basis for the detection mechanism.

1.7 References

[1] *What it is and how it works*. Retrieved on 5 Jun. 2019 from https://www.nano.gov/nanotech-101/what, June 2019.

[2] Feynman, R. P. There's plenty of room at the bottom. *Engineering and Science*, 23(5):22-36, 1960.

[3] Drexler, K. E. *Engines of Creation*. Anchor Press, New York, 1986.

[4] Kroto, H. W., Heath, J. R., O'Brien, S. C., Curl, R. F., and Smalley, R. E. C_{60}: Buckminsterfullerene. *Nature*, 318(6042):162-163, 1985.

[5] Iijima, S. Helical microtubules of graphitic carbon. *Nature*, 354(6348):56-58, 1991.

[6] Novoselov, K. S., Geim, A. K., Morozov, S. V., Jiang, D., Zhang, Y., Dubonos, S. V., Grigorieva, I. V., Firsov, A. A., Katsnelson, M. I., Geim, A. K., and Novoselov, K. S. Electric field effect in atomically thin carbon films. *Science*, 306(5696):666-669, 2004.

[7] Gwon, H., Kim, H.-S., Lee, K. U., Seo, D.-H., Park, Y. C., Lee, Y.-S., Ahn, B. T., and Kang, K. Flexible energy storage devices based on graphene paper. *Energy & Environmental Science*, 4(4):1277, 2011.

[8] Gomez De Arco, L., Zhang, Y., Schlenker, C. W., Ryu, K., Thompson, M. E., and Zhou, C. Continuous, highly flexible, and transparent graphene films by chemical vapor deposition for organic photovoltaics. *ACS Nano*, 4(5):2865-2873, 2010.

[9] Wang, S., Ang, P. K., Wang, Z., Tang, A. L. L., Thong, J. T. L., and Loh, K. P. High mobility, printable, and solution-processed graphene electronics. *Nano Letters*, 10(1):92-98, 2010.

[10] Graham, A. P., Duesberg, G. S., Hoenlein, W., Kreupl, F., Liebau, M., Martin, R., Rajasekharan, B., Pamler, W., Seidel, R., Steinhoegl, W., and Unger, E. How do carbon nanotubes fit into the semiconductor roadmap? *Applied Physics A: Materials Science and Processing*, 80(6):1141-1151, 2005.

[11] Zhang, J., Cheng, Y., Lee, Y. Z., Gao, B., Qiu, Q., Lin, W. L., Lalush, D., Lu, J. P., and Zhou, O. A nanotube-based field emission X-ray source for microcomputed tomography. *Review of Scientific Instruments*, 76(9):094301, 2005.

[12] Namdari, P., Negahdari, B., and Eatemadi, A. Synthesis, properties and biomedical applications of carbon-based quantum dots: An updated review. *Biomedicine & Pharmacotherapy*, 87:209-222, 2017.

[13] Jäger, H., Frohs, W., Collin, G., von Sturm, F., Vohler, O., and Nutsch, G. Carbon, 1. General. In *Ullmann's Encyclopedia of Industrial Chemistry*, pages 695-702, ISBN:9783527306732. Wiley-VCH Verlag GmbH & Co. KGaA, Weinheim, Germany, 2010.

[14] *Pigments through the Ages - Prehistory*. Retrieved on 5 Jun. 2019 from

http://www.webexhibits.org/pigments/intro/early.html, June 2019.

[15] Kelly, B. T. *Physics of graphite*. Applied Science, London, Englewood, N.J., 1981.

[16] Kotz, J. C., Treichel, P., and Townsend, J. R. *Chemistry & chemical reactivity*. Thomson Brooks/ Cole, Canada, 7th edition, 2008.

[17] Hirsch, A. The era of carbon allotropes. *Nature Materials*, 9(11):868-871, 2010.

[18] Krätschmer, W., Lamb, L. D., Fostiropoulos, K., and Huffman, D. R. Solid C_{60}: A new form of carbon. *Nature*, 347(6291):354-358, 1990.

[19] Zieleniewska, A., Lodermeyer, F., Roth, A., and Guldi, D. M. Fullerenes – How 25 years of charge transfer chemistry have shaped our understanding of (interfacial) interactions. *Chemical Society Reviews*, 47(3):702-714, 2018.

[20] Yang, H., Beavers, C. M., Wang, Z., Jiang, A., Liu, Z., Jin, H., Mercado, B. Q., Olmstead, M. M., and Balch, A. L. Isolation of a small carbon nanotube: The surprising appearance of $D_{5h}(1)$-C_{90}. *Angewandte Chemie*, 122(5):898-902, 2010.

[21] Nimibofa, A., Newton, E. A., Cyprain, A. Y., and Donbebe, W. Fullerenes: Synthesis and applications. *Journal of Materials Science Research*, 7(3):22-36, 2018.

[22] Geckeler, K. E. and Samal, S. Syntheses and properties of macromolecular fullerenes, a review. *Polymer International*, 48(9):743-757, 1999.

[23] Montellano López, A., Mateo-Alonso, A., and Prato, M. Materials chemistry of fullerene C_{60} derivatives. *Journal of Materials Chemistry*, 21(5):1305-1318, 2011.

[24] Ajie, H., Alvarez, M. M., Anz, S. J., Beck, R. D., Diederich, F., Fosliropoulos, K., Huffman, D. R., Kratschmer, W., Rubin, Y., Schriver, K. E., Sensharma, D., and Whetten, R. L. Characterization of the soluble all-carbon molecules C_{60} and C_{70}. *The Journal of Physical Chemistry*, 94:8630-8633, 1990.

[25] Boorum, M. M., Vasil'ev, Y. V, Drewello, T., and Scott, L. T. Groundwork for a rational synthesis of C_{60}: Cyclodehydrogenation of a $C_{60}H_{30}$ polyarene. *Science*, 294(5543):828-831, 2001.

[26] Demczyk, B. G., Wang, Y. M., Cumings, J., Hetman, M., Han, W., Zettl, A., and Ritchie, R. Direct mechanical measurement of the tensile strength and elastic modulus of multiwalled carbon nanotubes. *Materials Science and Engineering: A*, 334(1):173-178, 2002.

[27] Chang, C.-C., Hsu, I.-K., Aykol, M., Hung, W.-H., Chen, C.-C., and Cronin, S. B. A new lower limit for the ultimate breaking strain of carbon nanotubes. *ACS Nano*, 4(9):5095-5100, 2010.

[28] Wang, P., Xiang, R., and Maruyama, S. Thermal conductivity of carbon nanotubes and assemblies. 2018. DOI: 10.1016/bs.aiht.2018.07.004.

[29] *File: Types of carbon nanotubes.png - Wikipedia*. Retrieved on 5 Jun. 2019 from

https://en.wikipedia.org/wiki/File:Types_of_Carbon_Nanotubes.png, June 2019.

[30] *Multiwalled carbon nanotube 3ds*. Retrieved on 5 Jun. 2019 from https://www.turbosquid.com/3d-models/multiwalled-carbon-nanotube-3ds/363229, June 2019.

[31] Ebbesen, T. W. and Ajayan, P. M. Large-scale synthesis of carbon nanotubes. *Nature*, 358(6383):220-222, 1992.

[32] José-Yacamán, M., Miki-Yoshida, M., Rendón, L., and Santiesteban, J. G. Catalytic growth of carbon microtubules with fullerene structure. *Applied Physics Letters*, 62(6):657-659, 1993.

[33] Guo, T., Nikolaev, P., Rinzler, A. G., Tomdnek, D., Colbert, D. T., and Smalley, R. E. Self-assembly of tubular fullerenes. *The Journal of Physical Chemistry*, 99:10694-10697, 1995.

[34] Geim, A. K. and Novoselov, K. S. The rise of graphene. *Nature Materials*, 6(3):183-191, 2007.

[35] Novoselov, K. S., Morozov, S. V, Mohinddin, T. M. G., Ponomarenko, L. A., Elias, D. C., Yang, R., Barbolina, I. I., Blake, P., Booth, T. J., Jiang, D., Giesbers, J., Hill, E. W., and Geim, A. K. Electronic properties of graphene. *physica status solidi (b)*, 244(11):4106-4111, 2007.

[36] Terrones, M., Botello-Méndez, A. R., Campos-Delgado, J., López-Urías, F., Vega-Cantú, Y. I., Rodríguez-Macías, F. J., Elías, A. L., Muñoz-Sandoval, E., Cano-Márquez, A. G., and Charlier, J.-C. Graphene and graphite nanoribbons: Morphology, properties, synthesis, defects and applications. *Nano Today*, 5(4):351-372, 2010.

[37] Zhang, Y., Tang, T.-T., Girit, C., Hao, Z., Martin, M. C., Zettl, A., Crommie, M. F., Shen, Y. R., and Wang, F. Direct observation of a widely tunable bandgap in bilayer graphene. *Nature*, 459(7248):820-823, 2009.

[38] Partoens, B. and Peeters, F. M. From graphene to graphite: Electronic structure around the K point. *Physical Review B*, 74(7):075404, 2006.

[39] Bolotin, K. I., Sikes, K. J., Jiang, Z., Klima, M., Fudenberg, G., Hone, J., Kim, P., and Stormer, H. L. Ultrahigh electron mobility in suspended graphene. *Solid State Communications*, 146(9-10):351-355, 2008.

[40] Balandin, A. A., Ghosh, S., Bao, W., Calizo, I., Teweldebrhan, D., Miao, F., and Lau, C. N. Superior thermal conductivity of single-layer graphene. *Nano Letters*, 8(3):902-907, 2008.

[41] Lee, C., Wei, X., Kysar, J. W., and Hone, J. Measurement of the elastic properties and intrinsic strength of monolayer graphene. *Science*, 321(5887):385-388, 2008.

[42] de La Fuente, J. *Properties of graphene – Graphenea*. Retrieved on 5 Jun. 2019 from

https://www.graphenea.com/pages/graphene-properties#.XFRHpVUzbIU, June 2019.

[43] Ci, L., Song, L., Jariwala, D., ElÃ-as, A. L., Gao, W., Terrones, M., and Ajayan, P. M. Graphene shape control by multistage cutting and transfer. *Advanced Materials*, 21(44):4487-4491, 2009.

[44] Liang, X., Chang, A. S. P., Zhang, Y., Harteneck, B. D., Choo, H., Olynick, D. L., and Cabrini, S. Electrostatic force assisted exfoliation of prepatterned few-layer graphenes into device sites. *Nano Letters*, 9(1):467-472, 2009.

[45] Hiura, H., Ebbesen, T. W., Fujita, J., Tanigaki, K., and Takada, T. Role of sp^3 defect structures in graphite and carbon nanotubes. *Nature*, 367(6459):148-151, 1994.

[46] Chen, G., Weng, W., Wu, D., Wu, C., Lu, J., Wang, P., and Chen, X. Preparation and characterization of graphite nanosheets from ultrasonic powdering technique. *Carbon*, 42(4):753-759, 2004.

[47] Choucair, M., Thordarson, P., and Stride, J. A. Gram-scale production of graphene based on solvothermal synthesis and sonication. *Nature Nanotechnology*, 4(1):30-33, 2009.

[48] Liu, Z., Lin, L., Ren, H., and Sun, X. CVD synthesis of graphene. In *Thermal Transport in Carbon-Based Nanomaterials*, pages 19-56, ISBN:9780323462402. Elsevier, 2017.

[49] Huang, H., Chen, S., Wee, A. T. S., and Chen, W. Epitaxial growth of graphene on silicon carbide (SiC). In *Graphene*, pages 3-26, ISBN:9780857095084. Woodhead Publishing, 2014.

[50] Warner, J. H., Schäffel, F., Bachmatiuk, A., Rümmeli, M. H., Warner, J. H., Schäffel, F., Bachmatiuk, A., and Rümmeli, M. H. Properties of graphene. In *Graphene*, pages 61-127, ISBN:9780123945938. Elsevier, 2013.

[51] Elias, D. C., Nair, R. R., Mohiuddin, T. M. G., Morozov, S. V, Blake, P., Halsall, M. P., Ferrari, A. C., Boukhvalov, D. W., Katsnelson, M. I., Geim, A. K., and Novoselov, K. S. Control of graphene's properties by reversible hydrogenation: Evidence for graphane. *Science*, 323(5914):610-613, 2009.

[52] Osuna, S., Torrent-Sucarrat, M., Solà, M., Geerlings, P., Ewels, C. P., and Lier, G. Van Reaction mechanisms for graphene and carbon nanotube fluorination. *The Journal of Physical Chemistry C*, 114(8):3340-3345, 2010.

[53] Lerf, A., He, H., Forster, M., and Klinowski, J. Structure of graphite oxide revisited. *The Journal of Physical Chemistry B*, 102(23):4477-4482, 2002.

[54] Raidongia, K., Tan, A. T. L., and Huang, J. Graphene oxide: Some new insights into an old material. In *Carbon Nanotubes and Graphene*, pages 341-374, ISBN:9780080982328. Elsevier, 2014.

[55] Brodie, B. C. On the atomic weight of graphite. *Philosophical Transactions of the Royal Society of London*, 149:249-259, 1859.

[56] Staudenmaier, L. Verfahren zur darstellung der graphitsäure. *Berichte der deutschen chemischen Gesellschaft*, 31(2):1481-1487, 1898.

[57] Hummers Jr, W. S. and Offeman, R. E. Preparation of graphitic oxide. *Journal of the American Chemical Society*, 80:1339-1339, 1958.

[58] Stankovich, S., Dikin, D. A., Piner, R. D., Kohlhaas, K. A., Kleinhammes, A., Jia, Y., Wu, Y., Nguyen, S. T., and Ruoff, R. S. Synthesis of graphene-based nanosheets via chemical reduction of exfoliated graphite oxide. *Carbon*, 45(7):1558-1565, 2007.

[59] Muda, M. R., Ramli, M. M., Isa, S. S. M., Jamlos, M. F., Murad, S. A. Z., Norhanisah, Z., Isa, M. M., Kasjoo, S. R., Ahmad, N., Nor, N. I. M., and Khalid, N. Fundamental study of reduction graphene oxide by sodium borohydride for gas sensor application. *AIP Conference Proceedings*, 1808:020034, 2017.

[60] Schniepp, H. C., Car, R., Liu, J., Aksay, I. A., Li, J.-L., Abdala, A. A., Herrera-Alonso, M., Adamson, D. H., Prud'homme, R. K., McAllister, M. J., and Milius, D. L. Single sheet functionalized graphene by oxidation and thermal expansion of graphite. *Chemistry of Materials*, 19(18):4396-4404, 2007.

[61] Wang, C., Zhou, J., and Du, F. Synthesis of highly reduced graphene oxide for supercapacitor. *Journal of Nanomaterials*, 2016:1-7, 2016.

[62] Kistler, S. S. Coherent expanded aerogels and jellies. *Nature*, 127(3211):741-741, 1931.

[63] Sun, H., Xu, Z., and Gao, C. Multifunctional, ultra-flyweight, synergistically assembled carbon aerogels. *Advanced Materials*, 25(18):2554-2560, 2013.

[64] Gorgolis, G. and Galiotis, C. Graphene aerogels: A review. *2D Materials*, 4(3):032001, 2017.

[65] Kotal, M., Kim, J., Oh, J., and Oh, I.-K. Recent progress in multifunctional graphene aerogels. *Frontiers in Materials*, 3:29, 2016.

[66] Fang, Q., Shen, Y., and Chen, B. Synthesis, decoration and properties of three-dimensional graphene-based macrostructures: A review. *Chemical Engineering Journal*, 264:753-771, 2015.

[67] Qin, S.-Y., Liu, X.-J., Zhuo, R.-X., and Zhang, X.-Z. Microstructure-controllable graphene oxide hydrogel film based on a pH-responsive graphene oxide hydrogel. *Macromolecular Chemistry and Physics*, 213(19):2044-2051, 2012.

[68] Xu, Y., Sheng, K., Li, C., and Shi, G. Self-assembled graphene hydrogel via a one-step hydrothermal process. *ACS Nano*, 4(7):4324-4330, 2010.

[69] Sheng, K. X., Xu, Y. X., Li, C., and Shi, G. Q. High-performance self-assembled graphene hydrogels prepared by chemical reduction of graphene oxide. *New Carbon Materials*, 26(1):9-15, 2011.

[70] Huang, W., Ma, Y., Jiang, X., Li, J., and Fan, Q. Self-assembly of reduced graphene

oxide into three-dimensional architecture by divalent ion linkage. *The Journal of Physical Chemistry C*, 114(51):22462-22465, 2010.

[71] Fang, Q. and Chen, B. Self-assembly of graphene oxide aerogels by layered double hydroxides cross-linking and their application in water purification. *Journal of Materials Chemistry A*, 2(23):8941-8951, 2014.

[72] Adhikari, B., Biswas, A., and Banerjee, A. Graphene oxide-based hydrogels to make metal nanoparticle-containing reduced graphene oxide-based functional hybrid hydrogels. *ACS Applied Materials and Interfaces*, 4(10):5472-5482, 2012.

[73] Hong, J. Y., Bak, B. M., Wie, J. J., Kong, J., and Park, H. S. Reversibly compressible, highly elastic, and durable graphene aerogels for energy storage devices under limiting conditions. *Advanced Functional Materials*, 25(7):1053-1062, 2015.

[74] Zhao, Y., Cheng, H., Hu, C., Shi, G., Hu, Y., and Qu, L. A Versatile, ultralight, nitrogen-doped graphene framework. *Angewandte Chemie International Edition*, 51(45):11371-11375, 2012.

[75] Worsley, M. A., Pauzauskie, P. J., Olson, T. Y., Biener, J., Satcher, J. H., and Baumann, T. F. Synthesis of graphene aerogel with high electrical conductivity. *Journal of the American Chemical Society*, 132(40):14067-14069, 2010.

[76] Chen, Z., Ren, W., Gao, L., Liu, B., Pei, S., and Cheng, H.-M. Three-dimensional flexible and conductive interconnected graphene networks grown by chemical vapour deposition. *Nature Materials*, 10(6):424-428, 2011.

[77] Kim, B.-J., Yang, G., Joo Park, M., Seop Kwak, J., Hyeon Baik, K., Kim, D., and Kim, J. Three-dimensional graphene foam-based transparent conductive electrodes in GaN-based blue light-emitting diodes. *Applied Physics Letters*, 102(16):161902, 2013.

[78] Ho, M. P. and Lau, A. K.-T. Amorphous carbon nanocomposites. In *Fillers and Reinforcements for Advanced Nanocomposites*, pages 309-328, ISBN:9780081000793. Woodhead Publishing, 2015.

[79] Accorsi, J. and Yu, M. Carbon black. In Pritchard G, editor, *Plastics Additives*, pages 153-161, ISBN:9789401158626. Springer, Dordrecht, 1998.

[80] Pantea, D., Darmstadt, H., Kaliaguine, S., and Roy, C. Electrical conductivity of conductive carbon blacks: Influence of surface chemistry and topology. *Applied Surface Science*, 217(1):181-193, 2003.

[81] Tuerhong, M., Xu, Y., and Yin, X. B. Review on carbon dots and their applications. *Chinese Journal of Analytical Chemistry*, 45(1):139-150, 2017.

[82] Xu, X., Ray, R., Gu, Y., Ploehn, H. J., Gearheart, L., Raker, K., and Scrivens, W. A. Electrophoretic analysis and purification of fluorescent single-walled carbon nanotube fragments. *Journal of the American Chemical Society*, 126(40):12736-12737, 2004.

[83] Cayuela, A., Soriano, M. L., Carrillo-Carrión, C., and Valcárcel, M. Semiconductor and carbon-based fluorescent nanodots: The need for consistency. *Chemical Communications*, 52(7):1311-1326, 2016.

[84] Zhu, S., Song, Y., Zhao, X., Shao, J., Zhang, J., and Yang, B. The photoluminescence mechanism in carbon dots (graphene quantum dots, carbon nanodots, and polymer dots): Current state and future perspective. *Nano Research*, 8(2):355-381, 2015.

[85] Demchenko, A. P. and Dekaliuk, M. O. Novel fluorescent carbonic nanomaterials for sensing and imaging. *Methods and Applications in Fluorescence*, 1(4):042001, 2013.

[86] Li, H., He, X., Kang, Z., Huang, H., Liu, Y., Liu, J., Lian, S., Tsang, C. H. A., Yang, X., and Lee, S. T. Water-soluble fluorescent carbon quantum dots and photocatalyst design. *Angewandte Chemie - International Edition*, 49(26):4430-4434, 2010.

[87] Meziani, M. J., Lin, Y., Wang, X., Murray, D., Xie, S.-Y., Wang, H., Veca, L. M., Luo, P. G., Harruff, B. A., Cao, L., Sun, Y.-P., and Lu, F. Carbon dots for multiphoton bioimaging. *Journal of the American Chemical Society*, 129(37):11318-11319, 2007.

[88] Wang, J., Wang, C. F., and Chen, S. Amphiphilic egg-derived carbon dots: Rapid plasma fabrication, pyrolysis process, and multicolor printing patterns. *Angewandte Chemie - International Edition*, 51(37):9297-9301, 2012.

[89] Lu, W., Luo, Y., Zhang, Y., Asiri, A. M., Liu, S., Qin, X., Chang, G., Al-Youbi, A. O., and Sun, X. Economical, green synthesis of fluorescent carbon nanoparticles and their use as probes for sensitive and selective detection of mercury(II) ions. *Analytical Chemistry*, 84(12):5351-5357, 2012.

[90] Zheng, J. X., Liu, X. H., Yang, Y. Z., Liu, X. G., and Xu, B. S. Rapid and green synthesis of fluorescent carbon dots from starch for white light-emitting diodes. *New Carbon Materials*, 33(3):276-288, 2018.

[91] Zhu, S., Meng, Q., Wang, L., Zhang, J., Song, Y., Jin, H., Zhang, K., Sun, H., Wang, H., and Yang, B. Highly photoluminescent carbon dots for multicolor patterning, sensors, and bioimaging. *Angewandte Chemie - International Edition*, 52(14):3953-3957, 2013.

[92] Li, H., He, X., Liu, Y., Huang, H., Lian, S., Lee, S.-T., and Kang, Z. One-step ultrasonic synthesis of water-soluble carbon nanoparticles with excellent photoluminescent properties. *Carbon*, 49(2):605-609, 2010.

[93] Zhu, H., Wang, X., Li, Y., Wang, Z., Yang, F., and Yang, X. Microwave synthesis of fluorescent carbon nanoparticles with electrochemiluminescence properties. *Chemical Communications*, 0(34):5118-5120, 2009.

[94] Mittal, V. Polymer nanocomposites: Synthesis, microstructure, and properties. In *Optimization of Polymer Nanocomposite Properties*, pages 1-19, Wiley-VCH Verlag GmbH & Co. KGaA, Weinheim, Germany, 2010.

[95] Suckeveriene, R. Y., Zelikman, E., Mechrez, G., and Narkis, M. Literature review: Conducting carbon nanotube/polyaniline nanocomposites. *Reviews in Chemical Engineering*, 27:15-21, 2011.

[96] Epstein, A. J., Ginder, J. M., Zuo, F., Bigelow, R. W., Woo, H.-S., Tanner, D. B., Richter, A. F., Huang, W.-S., and Macdiarmid, A. G. Insulator-to-metal transition in polyaniline. *Synthetic Metals*, 18:303-309, 1987.

[97] Bhowmik, K. L., Deb, K., Bera, A., Nath, R. K., and Saha, B. Charge transport through polyaniline incorporated electrically conducting functional paper. *The Journal of Physical Chemistry C*, 120(11):5855-5860, 2016.

[98] Malhotra, B. D. Defects in conducting polymers. *Bulletin of Materials Science*, 10:85-96, 1988.

[99] Tan, C., Huang, X., and Zhang, H. Synthesis and applications of graphene-based noble metal nanostructures. *Materials Today*, 16:29-36, 2013.

[100] Khan, M., Tahir, M. N., Adil, S. F., Khan, H. U., Siddiqui, M. R. H., Al-Warthan, A. A., and Tremel, W. Graphene based metal and metal oxide nanocomposites: Synthesis, properties and their applications. *Journal of Materials Chemistry A*, 3(37):18753-18808, 2015.

[101] Ghosh, S. and Das, A. P. Modified titanium oxide (TiO_2) nanocomposites and its array of applications: A review. *Toxicological & Environmental Chemistry*, 97(5):491-514, 2015.

[102] Ray, C. and Pal, T. Recent advances of metal-metal oxide nanocomposites and their tailored nanostructures in numerous catalytic applications. *Journal of Materials Chemistry A*, 5(20):9465-9487, 2017.

[103] Zhang, T., Mubeen, S., Myung, N. V, and Deshusses, M. A. Recent progress in carbon nanotube-based gas sensors. *Nanotechnology*, 19(33):332001, 2008.

[104] Wang, Y. and Yeow, J. T. W. A review of carbon nanotubes-based gas sensors. *Journal of Sensors*, 2009:1-24, 2009.

[105] Mirica, K. A., Weis, J. G., Schnorr, J. M., Esser, B., and Swager, T. M. Mechanical drawing of gas sensors on paper. *Angewandte Chemie - International Edition*, 51(43):10740-10745, 2012.

[106] Kong, J., Franklin, N. R., Zhou, C., Chapline, M. G., Peng, S., Cho, K., and Dai, H. Nanotube molecular wires as chemical sensors. *Science*, 287(5453):622-625, 2000.

[107] Kong, J., Chapline, M. G., and Dai, H. Functionalized carbon nanotubes for molecular hydrogen sensors. *Advanced Materials*, 13(18):1384-1386, 2001.

[108] Collins, P. G., Bradley, K., Ishigami, M., and Zettl, A. Extreme oxygen sensitivity of electronic properties of carbon nanotubes. *Science*, 287(5459):1801-1804, 2000.

[109] Kauffman, D. R., Sorescu, D. C., Schofield, D. P., Allen, B. L., Jordan, K. D., and Star,

A. Understanding the sensor response of metal-decorated carbon nanotubes. *Nano Letters*, 10(3):958-963, 2010.

[110] Yoo, K.-P., Kwon, K.-H., Min, N.-K., Lee, M. J., and Lee, C. J. Effects of O_2 plasma treatment on NH_3 sensing characteristics of multiwall carbon nanotube/polyaniline composite films. *Sensors and Actuators B: Chemical*, 143(1):333-340, 2009.

[111] Lee, K., Lee, J. W., Kim, S. Il, and Ju, B. K. Single-walled carbon nanotube/Nafion composites as methanol sensors. *Carbon*, 49(3):787-792, 2011.

[112] Lu, G., Ocola, L. E., and Chen, J. Reduced graphene oxide for room-temperature gas sensors. *Nanotechnology*, 20(44):445502, 2009.

[113] Wu, J., Feng, S., Wei, X., Shen, J., Lu, W., Shi, H., Tao, K., Lu, S., Sun, T., Yu, L., Du, C., Miao, J., and Norford, L. K. Facile synthesis of 3D graphene flowers for ultrasensitive and highly reversible gas sensing. *Advanced Functional Materials*, 26(41):7462-7469, 2016.

[114] Schedin, F., Geim, A. K., Morozov, S. V., Hill, E. W., Blake, P., Katsnelson, M. I., and Novoselov, K. S. Detection of individual gas molecules adsorbed on graphene. *Nature Materials*, 6(9):652-655, 2007.

[115] Dan, Y., Lu, Y., Kybert, N. J., Luo, Z., and Johnson, A. T. C. Intrinsic response of graphene vapor sensors. *Nano Letters*, 9(4):1472-1475, 2009.

[116] Jung, I., Dikin, D., Park, S., Cai, W., Mielke, S. L., and Ruoff, R. S. Effect of water vapor on electrical properties of individual reduced graphene oxide sheets. *The Journal of Physical Chemistry C*, 112(51):20264-20268, 2008.

[117] Kauffman, D. R. and Star, A. Graphene versus carbon nanotubes for chemical sensor and fuel cell applications. *Analyst*, 135(11):2790-2797, 2010.

[118] Liu, C., Tang, B., Zhang, S., Zhou, M., Yang, M., Liu, Y., Zhang, Z. L., Zhang, B., and Pang, D. W. Photoinduced electron transfer mediated by coordination between carboxyl on carbon nanodots and Cu^{2+} quenching photoluminescence. *The Journal of Physical Chemistry C*, 122(6):3662-3668, 2018.

[119] Shi, Y., Li, C., Liu, S., Liu, Z., Zhu, J., Yang, J., and Hu, X. Facile synthesis of fluorescent carbon dots for determination of curcumin based on fluorescence resonance energy transfer. *RSC Advances*, 5(79):64790-64796, 2015.

[120] Rong, M., Lin, L., Song, X., Zhao, T., Zhong, Y., Yan, J., Wang, Y., and Chen, X. A label-free fluorescence sensing approach for selective and sensitive detection of 2,4,6-trinitrophenol (TNP) in aqueous solution using graphitic carbon nitride nanosheets. *Analytical Chemistry*, 87(2):1288-1296, 2015.

[121] Dong, Y., Wang, R., Li, G., Chen, C., Chi, Y., and Chen, G. Polyamine-functionalized carbon quantum dots as fluorescent probes for selective and sensitive detection of copper

ions. *Analytical Chemistry*, 84(14):6220-6224, 2012.

[122] Zheng, M., Xie, Z., Qu, D., Li, D., Du, P., Jing, X., and Sun, Z. On-off-on fluorescent carbon dot nanosensor for recognition of chromium(VI) and ascorbic acid based on the inner filter effect. *ACS Applied Materials and Interfaces*, 5(24):13242-13247, 2013.

[123] Jiang, Y., Wang, Y., Meng, F., Wang, B., Cheng, Y., and Zhu, C. N-doped carbon dots synthesized by rapid microwave irradiation as highly fluorescent probes for Pb^{2+} detection. *New Journal of Chemistry*, 39(5):3357-3360, 2015.

[124] Li, Z., Yu, H., Bian, T., Zhao, Y., Zhou, C., Shang, L., Liu, Y., Wu, L. Z., Tung, C. H., and Zhang, T. Highly luminescent nitrogen-doped carbon quantum dots as effective fluorescent probes for mercuric and iodide ions. *Journal of Materials Chemistry C*, 3(9):1922-1928, 2015.

[125] Yin, B., Deng, J., Peng, X., Long, Q., Zhao, J., Lu, Q., Chen, Q., Li, H., Tang, H., Zhang, Y., and Yao, S. Green synthesis of carbon dots with down- and up-conversion fluorescent properties for sensitive detection of hypochlorite with a dual-readout assay. *Analyst*, 138(21):6551-6557, 2013.

[126] Gao, X., Ding, C., Zhu, A., and Tian, Y. Carbon-dot-based ratiometric fluorescent probe for imaging and biosensing of superoxide anion in live cells. *Analytical Chemistry*, 86(14):7071-7078, 2014.

[127] Wang, Q., Liu, X., Zhang, L., and Lv, Y. Microwave-assisted synthesis of carbon nanodots through an eggshell membrane and their fluorescent application. *Analyst*, 137(22):5392-5397, 2012.

[128] Jana, J., Ganguly, M., and Pal, T. Intriguing cysteine induced improvement of the emissive property of carbon dots with sensing applications. *Physical Chemistry Chemical Physics*, 17(4):2394-2403, 2015.

[129] Shen, P. and Xia, Y. Synthesis-modification integration: One-step fabrication of boronic acid functionalized carbon dots for fluorescent blood sugar sensing. *Analytical Chemistry*, 86(11):5323-5329, 2014.

[130] Lan, M., Di, Y., Zhu, X., Ng, T. W., Xia, J., Liu, W., Meng, X., Wang, P., Lee, C. S., and Zhang, W. A carbon dot-based fluorescence turn-on sensor for hydrogen peroxide with a photo-induced electron transfer mechanism. *Chemical Communications*, 51(85):15574-15577, 2015.

[131] Sun, X., He, J., Meng, Y., Zhang, L., Zhang, S., Ma, X., Dey, S., Zhao, J., and Lei, Y. Microwave-assisted ultrafast and facile synthesis of fluorescent carbon nanoparticles from a single precursor: Preparation, characterization and their application for the highly selective detection of explosive picric acid. *Journal of Materials Chemistry A*, 4(11):4161-4171, 2016.

[132] *Becquerel prize for outstanding merits in photovoltaics: Alexandre Edmond Becquerel*. Retrieved on 5 Jun. 2019 from https://www.becquerel-prize.org/about-the-becquerel-prize/alexandre-edmond-becquerel/, June 2019.

[133] O'Regan, B. and Grätzel, M. A low-cost, high-efficiency solar cell based on dye-sensitized colloidal TiO_2 films. *Nature*, 353(6346):737-740, 1991.

[134] Kakiage, K., Aoyama, Y., Yano, T., Oya, K., Fujisawa, J. I., and Hanaya, M. Highly-efficient dye-sensitized solar cells with collaborative sensitization by silyl-anchor and carboxy-anchor dyes. *Chemical Communications*, 51(88):15894-15897, 2015.

[135] Sharma, K., Sharma, V., and Sharma, S. S. Dye-sensitized solar cells: Fundamentals and current status. *Nanoscale Research Letters*, 13(1):381, 2018.

[136] Wu, J., Lan, Z., Lin, J., Huang, M., Huang, Y., Fan, L., and Luo, G. Electrolytes in dye-sensitized solar cells. *Chemical Reviews*, 115(5):2136-2173, 2015.

[137] Wu, J., Lan, Z., Lin, J., Huang, M., Huang, Y., Fan, L., Luo, G., Lin, Y., Xie, Y., and Wei, Y. Counter electrodes in dye-sensitized solar cells. *Chemical Society Reviews*, 46(19):5975-6023, 2017.

[138] Sigdel, S., Dubey, A., Elbohy, H., Aboagye, A., Galipeau, D., Zhang, L., Fong, H., and Qiao, Q. Dye-sensitized solar cells based on spray-coated carbon nanofiber/TiO_2 nanoparticle composite counter electrodes. *Journal of Materials Chemistry A*, 2(29):11448-11453, 2014.

[139] He, B., Meng, X., and Tang, Q. Low-cost counter electrodes from CoPt alloys for efficient dye-sensitized solar cells. *ACS Applied Materials and Interfaces*, 6(7):4812-4818, 2014.

[140] Tai, Q., Chen, B., Guo, F., Xu, S., Hu, H., Sebo, B., and Zhao, X. Z. In situ prepared transparent polyaniline electrode and its application in bifacial dye-sensitized solar cells. *ACS Nano*, 5(5):3795-3799, 2011.

[141] Hu, L. and Xu, K. Nonflammable electrolyte enhances battery safety. *Proceedings of the National Academy of Sciences*, 111(9):3205-3206, 2014.

[142] Kim, B. K., Sy, S., Yu, A., and Zhang, J. Electrochemical supercapacitors for energy storage and conversion. In Yan J, editor, *Handbook of Clean Energy Systems*, pages 1-25, ISBN:9781118991978. John Wiley & Sons, Ltd., 2015.

[143] Yang, H., Kannappan, S., Pandian, A. S., Jang, J. H., Lee, Y. S., and Lu, W. Graphene supercapacitor with both high power and energy density. *Nanotechnology*, 28(44):445401, 2017.

[144] Subramanian, V., Luo, C., Stephan, A. M., Nahm, K. S., Thomas, S., and Wei, B. Supercapacitors from activated carbon derived from banana fibers. *The Journal of Physical Chemistry C*, 111(20):7527-7531, 2007.

[145] Qian, H., Kucernak, A. R., Greenhalgh, E. S., Bismarck, A., and Shaffer, M. S. P. Multifunctional structural supercapacitor composites based on carbon aerogel modified high performance carbon fiber fabric. *ACS Applied Materials and Interfaces*, 5(13):6113-6122, 2013.

[146] An, K. H., Kim, W. S., Park, Y. S., Choi, Y. C., Lee, S. M., Chung, D. C., Bae, D. J., Lim, S. C., and Lee, Y. H. Supercapacitors using single-walled carbon nanotube electrodes. *Advanced Materials*, 13(7):497-500, 2001.

[147] Xie, X., Zhang, C., Wu, M.-B., Tao, Y., Lv, W., and Yang, Q.-H. Porous MnO_2 for use in a high performance supercapacitor: Replication of a 3D graphene network as a reactive template. *Chemical Communications*, 49(94):11092-11094, 2013.

[148] Ahn, Y. R., Park, C. R., Jo, S. M., and Kim, D. Y. Enhanced charge-discharge characteristics of RuO_2 supercapacitors on heat-treated TiO_2 nanorods. *Applied Physics Letters*, 90(12):122106, 2007.

[149] Vijayakumar, S., Nagamuthu, S., and Muralidharan, G. Supercapacitor studies on NiO nanoflakes synthesized through a microwave route. *ACS Applied Materials and Interfaces*, 5(6):2188-2196, 2013.

[150] Wu, Z., Zhu, Y., and Ji, X. $NiCo_2O_4$-based materials for electrochemical supercapacitors. *Journal of Materials Chemistry A*, 2(36):14759-14772, 2014.

[151] Li, L., Tan, L., Li, G., Zhang, Y., and Liu, L. Self-templated synthesis of porous $Ni(OH)_2$ nanocube and its high electrochemical performance for supercapacitor. *Langmuir*, 33(43):12087-12094, 2017.

[152] Shen, K., Ran, F., Zhang, X., Liu, C., Wang, N., Niu, X., Liu, Y., Zhang, D., Kong, L., Kang, L., and Chen, S. Supercapacitor electrodes based on nano-polyaniline deposited on hollow carbon spheres derived from cross-linked co-polymers. *Synthetic Metals*, 209:369-376, 2015.

[153] Lu, P., Ohlckers, P., and Chen, X. Y. On-chip supercapacitor electrode based on polypyrrole deposited into nanoporous Au scaffold. *Journal of Physics: Conference Series*, 773(1):012054, 2016.

[154] Iro, Z. S., Subramani, C., and Dash, S. S. A brief review on electrode materials for supercapacitor. *International Journal of Electrochemical Science*, 11(12):10628-10643, 2016.

[155] Muzaffar, A., Ahamed, M. B., Deshmukh, K., and Thirumalai, J. A review on recent advances in hybrid supercapacitors: Design, fabrication and applications. *Renewable and Sustainable Energy Reviews*, 101:123-145, 2019.

[156] Jurewicz, K., Delpeux, S., Bertagna, V., Béguin, F., and Frackowiak, E. Supercapacitors from nanotubes/polypyrrole composites. *Chemical Physics Letters*, 347:36-40, 2001.

[157] Fan, Z., Yan, J., Wei, T., Zhi, L., Ning, G., Li, T., and Wei, F. Asymmetric supercapacitors based on graphene/MnO_2 and activated carbon nanofiber electrodes with high power and energy density. *Advanced Functional Materials*, 21(12):2366-2375, 2011.

[158] Shao, Y., El-Kady, M. F., Sun, J., Li, Y., Zhang, Q., Zhu, M., Wang, H., Dunn, B., and Kaner, R. B. Design and mechanisms of asymmetric supercapacitors. *Chemical Reviews*, 118(18):9233-9280, 2018.

[159] Li, H., Cheng, L., and Xia, Y. A hybrid electrochemical supercapacitor based on a 5 V Li-ion battery cathode and active carbon. *Electrochemical and Solid-State Letters*, 8(9):A433, 2005.

[160] Kötz, R. and Carlen, M. Principles and applications of electrochemical capacitors. *Electrochimica Acta*, 45(15):2483-2498, 2000.

[161] Iwasita, T., Hoster, H., John-Anacker, A., Lin, W. F., and Vielstich, W. Methanol oxidation on PtRu electrodes. Influence of surface structure and Pt−Ru atom distribution. *Langmuir*, 16(2):522-529, 2002.

[162] Liu, H., Song, C., Zhang, L., Zhang, J., Wang, H., and Wilkinson, D. P. A review of anode catalysis in the direct methanol fuel cell. *Journal of Power Sources*, 155(2):95-110, 2006.

[163] Rao, V., Simonov, P. A., Savinova, E. R., Plaksin, G. V., Cherepanova, S. V., Kryukova, G. N., and Stimming, U. The influence of carbon support porosity on the activity of PtRu/Sibunit anode catalysts for methanol oxidation. *Journal of Power Sources*, 145(2):178-187, 2005.

[164] Panayotov, D. A., Burrows, S. P., and Morris, J. R. Photooxidation mechanism of methanol on rutile TiO_2 nanoparticles. *The Journal of Physical Chemistry C*, 116(11):6623-6635, 2012.

[165] Antolini, E. Photo-assisted methanol oxidation on Pt-TiO_2 catalysts for direct methanol fuel cells: A short review. *Applied Catalysis B: Environmental*, 237:491-503, 2018.